Redox Biol. 2024 Sep 24;77:103370. doi: 10.1016/j.redox.2024.103370

Over-activation of iNKT cells aggravate lung injury in bronchopulmonary dysplasia mice

Ming-Yan Wang [a,1], Meng-Xu Yi [a,1], Xing-Yu Mo [a], Shan-Jie Wei [a], Yu Qiao [a], Zheng Zhang [b], Zhao-Liang Su [b,c,**], Hong-Yan Lu [a,*]

Author information Article notes
PMCID: PMC11470607 PMID: 39342744

Abstract

Bronchopulmonary dysplasia (BPD) is a severe lung disease in preterm infants, the abnormal proliferate and differentiate ability of type II epithelial cells (AEC II) is the key to the pathological basis of BPD. Mechanisms regarding abnormal AEC II in BPD remain unclear. The present work investigated the role and mechanisms of invariant natural killer T (iNKT) cells in lung disorder in BPD using public datasets, clinical samples, a hyperoxia-induced BPD mouse model and AEC II-iNKT cells transwell co-culture system. Firstly, we found that the NKT cells development factor IL-15 increased over time in patients with BPD in public databases, and clinically collected peripheral blood NKT cells in patients with BPD were increased. Subsequently, the percentage of iNKT cells increased in hyperoxia group compared with normoxia group, with the highest at P7, accompanied by increased activation with abnormal lung development. The administration of anti-CD1d neutralizing antibody to inhibit iNKT cells could alleviate the abnormal lung development of hyperoxia group mice, while α-GalCer administration could aggravate lung injury in hyperoxia group mice, and adoptive transfer of iNKT cells could aggravate the abnormal lung development in hyperoxia group mice. In addition, to further verify the role of iNKT cells on AEC II, AEC II-iNKT cells co-culture system was established. The presence of iNKT cells could aggravate the abnormal expression of SP-C and T1α under hyperoxia.

Meanwhile, RNA-seq analysis showed that ferroptosis-related genes were highly expressed in AEC II co-cultured with iNKT cells under hyperoxia. We further validated the effect of the presence of iNKT cells under hyperoxia environment on AEC II ferroptosis levels, suggested that iNKT cells promote AEC II ferroptosis under hyperoxia, accompanied by decreased expression of SP-C and T1α. Our study found that the recruitment of iNKT cells in the lung may be an important cause of alveolarization disorder in BPD.

Keywords: Alveolar type II epithelial cells, Bronchopulmonary dysplasia, Differentiation, Invariant natural killer T cells, Ferroptosis

Graphical abstract

Hyperoxia exposure promotes recruitment or local expansion of activated iNKT cells in the lungs. Over-activated iNKT leads to increased ferroptosis in AEC II, accompanied by decreased expression of SP-C and T1α, AEC II dysfunction leads to the obstruction of alveolarization and occurrence of BPD. The figure was drawn online at Figuredraw (https://www.figdraw.com).

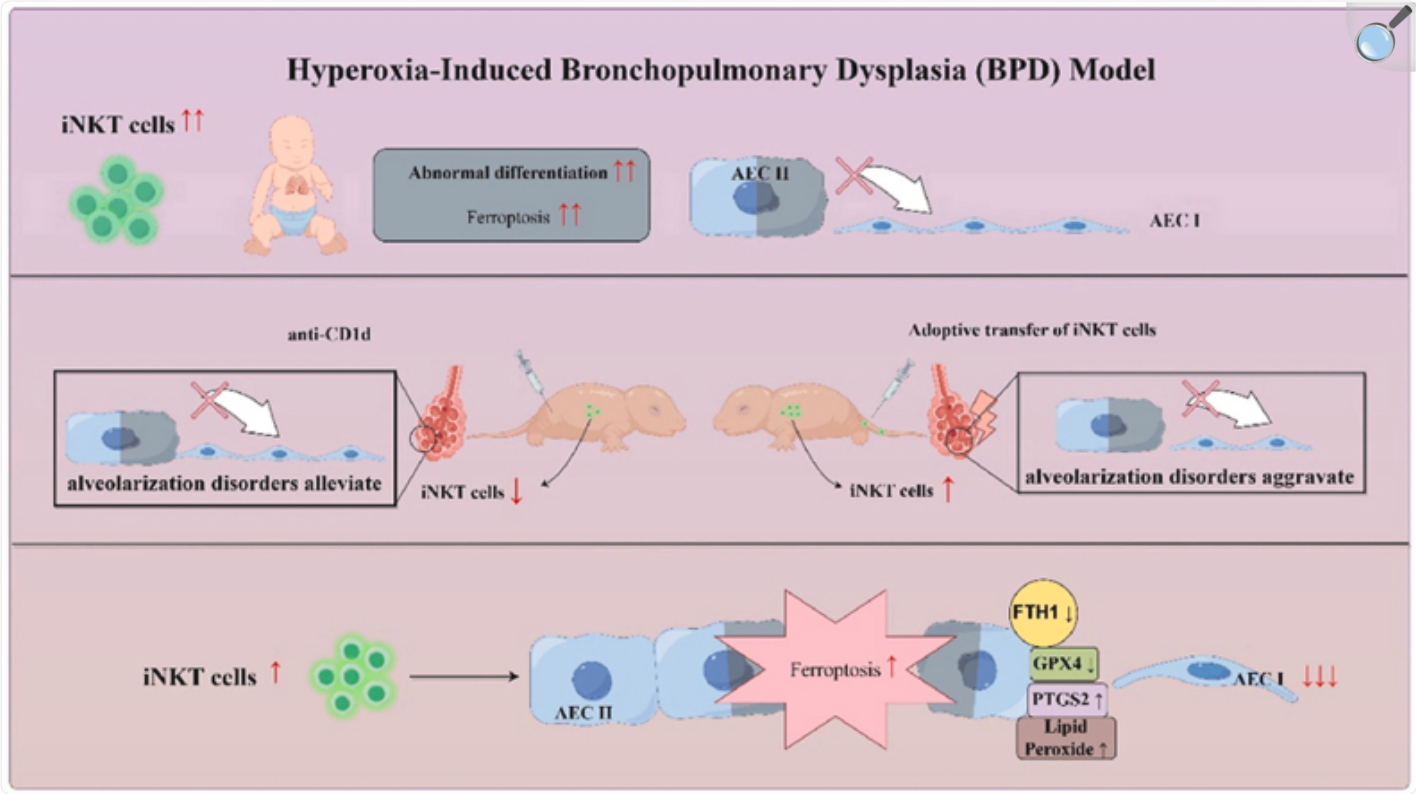

Open in a new tab

Highlights

- Hyperoxia leads to the recruitment and activation of iNKT cells in the lungs in BPD.
- Improvement of lung disorder with inhibition of iNKT cells activation and abundance in BPD.
- Over-activated iNKT cells induces ferroptosis in AEC II under hyperoxia, accompanied by decreased expression of SP-C and T1α.
- The abundance and over-activation of iNKT cells in the lung may be an important cause of alveolarization disorder in BPD.

1. Introduction

Bronchopulmonary dysplasia (BPD) is a severe lung disease characterized by immature lung development that affects almost half of extremely preterm infants [1]. Decreased alveolar number, simplified alveolar structure, and accompanying vascular lesions are features of BPD [2]. Hyperoxia can induce BPD phenotype and change the composition of cellular compartments [3]. Alveolar type II epithelial cells (AEC II) are the main stem cells of the lung and maintain normal lung function [4]. When the lung is damaged, AEC II have a role in replacing abnormal and damaged alveolar epithelial cells [5]. In particular, the abnormal ability of AEC II to proliferate and differentiate into AEC I is an important factor leading to this disease [6,7]. More and more evidence has shown that in addition to direct AEC II injury, other cell programmed cell death (PCD) including apoptosis [8], pyroptosis [9], autophagy [10] and ferroptosis [11] plays an important role in the molecular and biological mechanism of BPD and the further development of the disease [12]. Studies have shown that alveolar epithelial cell deaths are associated with lung injury, affecting alveolar development and participates in the pathological process of BPD [12]. Therefore, it is essential to explore the potential pathogenesis of AEC II in BPD for the development and treatment of BPD.

At present, many studies have focused on the regulation of the immune microenvironment during lung development and disease [13]. The pathogenesis of BPD also includes changes in the proportion of immune cells [9]. In recent years, studies have mainly focused on the role of immune cells and immune responses in the pathogenesis of BPD, but the mechanism and role of different immune cells in BPD still unclear. Several recent discoveries have been made regarding how a particular subset of Natural killer T (NKT) cells, invariant natural killer T (iNKT) cells, play a key role in chronic inflammation and fibrosis in lung [14] and liver diseases [15], iNKT cells activation is considered to be an important upstream event that promotes chronic pulmonary inflammation and fibrosis [15,16]. iNKT cells are considered as a kind of innate T lymphocyte population, which are lymphocytes with the characteristics of innate immune cells and adaptive immune cells, and serve as a bridge connecting the two immune responses, which can initiate or inhibit immune responses depending on the environment, account for the majority of NKT cells [17]. iNKT cells are tissue-resident and play an important role in tissue homeostasis and immunity in lung tissues, they patrol the lumen of pulmonary vascular and interstitial tissue until lung tissue becomes infected and signals danger, causing iNKT cells migrate to damaged sites containing glycolipid antigens and inducing iNKT cells to initiate early host defense mechanisms, preferentially locating

in lung parenchyma [18].

The percentage of iNKT cells in lung tissue was higher than that of other lymphocytes in the lung [19]. Previous studies have shown that the number and function of iNKT cells are different in different lung diseases [14]. Pulmonary iNKT cells are involved in the pathogenesis of various lung diseases, including direct pathogenic effects through their cytokine secretion, or more indirectly by regulating the function of neighboring immune cells [14]. In particular, cytokine production by iNKT cells has been implicated in many lung diseases, including allergic asthma [20], chronic obstructive pulmonary disease (COPD) [21], pulmonary fibrosis [16], acute respiratory distress syndrome (ARDS) [22], and others. iNKT cells are adaptive immune cells with innate functions that have been shown to play a role in the neonatal immune response, where they can be activated by proinflammatory cytokines or lipid antigens and trigger further cytokine production and activation by other immune cell populations [23]. It has been shown that iNKT cells play an important role in the neonatal response to sepsis, and loss of iNKT cells leads to improved survival in neonatal septic mice [24]. iNKT cells are involved in the deterioration of lung disease after respiratory syncytial virus (RSV) infection in neonatal mice [25]. Therefore, it may be particularly valuable to further investigate the role of pulmonary iNKT cells in respiratory diseases, which may facilitate the development of novel therapeutic targets. However, the role of iNKT cells in BPD remains unclear.

IL-15 is a major cytokine responsible for NKT cells development, maturation, and survival [26]. In this study, we first downloaded microarray data from GEO database to analyze the peripheral blood IL-15 expression in BPD patients, and clinically examined peripheral blood NKT cells changes in BPD patients. Secondly, a mouse model of BPD was established by hyperoxia to investigate the effect of iNKT cells in lung tissue on lung differentiation. Finally, iNKT cells sorted by magnetic beads and AEC II-iNKT cells transwell co-culture system were established in vitro under hyperoxia. Transcriptome sequencing was performed on AEC II under different incubation conditions to investigate the possible mechanisms by which iNKT cells affect AEC II.

2. Methods

2.1. Microarray analysis of the NKT cells developmental factor IL-15 in BPD

Since IL-15 is a major cytokine responsible for NKT cell development, maturation, and survival [26], we investigated changes in IL-15 expression in BPD patients. We screened the GEO database for microarray sequencing analysis data that met the following criteria: (1) studies containing preterm infants of less than 32 weeks gestational age and birth weight ≤1500 g, (2) studies with blood samples that were from infants on the 5th to 14th day of life for the assessment of gene expression. Based on the above criteria, one data set (GSE32472) [27] was obtained from the GEO database. A total of 111 preterm infants were included in this prospective study, conducted between September 1, 2008, and November 30, 2010. The GSE32472 of RNA sequencing in peripheral blood of BPD children was downloaded from

NCBI GEO database (https://www.ncbi.nlm.nih.gov/geo/). These data were normalized and $\log_2$ transformed. Analyses were performed using the GEO2R tool.

2.2. Flow cytometry was used to detect NKT cells in peripheral blood of BPD patients

Patients hospitalized in the Department of Pediatrics, Affiliated Hospital of Jiangsu University from September 2022 to January 2024, Twenty preterm infants (selected gestational age＜32 weeks and length of hospital stay＞14 d). Exclusion criteria: (1) complicated with severe congenital malformation; (2) combined with inherited metabolic diseases and/or chromosomal diseases; (3) withdrawal from treatment or death during hospitalization; (4) missing clinical data; (5) Informed consent was not obtained. According to the diagnostic criteria of BPD, they were divided into BPD group (n = 10) and non-BPD group (n = 10). BPD was diagnosed according to the 2018 BPD diagnostic criteria [28]. Whole blood (0.5 mL) was collected from the BPD patients and healthy controls using an anticoagulant tube, then 10 mL of ACK split red cell was added twice, and stained with CD45-PECy5.5, CD3 -FITC and CD56-PE (BioLegend, USA). NKT cells were labeled by $CD45^+CD3^+CD56^+$ cells [21,29,30]. The activation of NKT cells was assessed by CD69 [21]. The expression of $CD45^+CD3^+CD56^+$ and CD69 was detected by flow cytometry to observe the percentage and activation status of NKT cells. The basic information of the patient is shown in Table 1. This study was approved by the Biomedical Research Ethics Committee of Affiliated Hospital of Jiangsu University (SWYXLL20200121-17).

Table 1.

Basic information of the patient.

Characteristic	Non-BPD	BPD
Number of cases	10	10
Birth weight	1658 ± 172	1351 ± 184
Gestational age	30.7 ± 1.0	28.9 ± 1.0
Sex, male/female	5/5	7/3
Chronologic age of premature infants	31	32
History of chorioamnionitis	2	3
Early onset sepsis	1	3

Open in a new tab

2.3. Establishment of BPD models

Pregnant C57BL/6 mice were purchased from the Animal Center of Jiangsu University at embryonic day (E)15-E17. All pups were randomly assigned and allocated to two nursing mothers at P1 (P0 is the birth date) to obtain six or seven newborn mice per nursing mother. This study used a hyperoxia model: hyperoxia (85 % O_2) from P1 to P14 according to the model establishment method in the research group [31], and the nursing mother mice were replaced every 12 h to avoid oxygen poisoning. To exclude the effect of sex, we used male mice. Mice were housed in specific pathogen free (SPF) grade animal feeding facilities, and a self-made hyperoxia device and oxygen making machine (Yuyue, China) were used and the procedures were approved by the Institutional Animal Care and Use Committee of Jiangsu University (Grant no: UJS-IACUC-2022052501).

2.4. Pathological analysis and glycogen staining

The overall technique used in mouse lung acquisition and analysis has been previously published by our group [31]. In brief, at P3, P7, P10 and P14, lungs were thoroughly perfused with PBS before harvesting, part of the lung tissue in 4 % paraformaldehyde was used for paraffin embedding, and part of the lung was flash frozen for protein and RNA isolation.

All studies were performed in each experiment with 4–9 animals per group. Fixed tissue was cut into 5 μm thick sections and sections were used for hematoxylin-eosin (H&E) staining morphometric analysis. To obtain a complete slide image, the slide was scanned. Lung volume measurements were performed by carefully drying the inflated and fixed lungs with soft tissue and assessed using the Archimedes principle [3]. At least 5 slides were assessed under a light microscope at 100× magnification from per mouse of each specimen. Images were from 10 randomly selected parenchymal fields, and regions with large airways or blood vessels were excluded. The structural and morphological changes of the lung tissue were observed under a light microscope at 400× magnification. Radial alveolar count (RAC) and mean linear intercept (MLI) were obtained using previously described methods [32]. Periodic acid-Schiff (PAS) staining was processed and examined as previously described [33].

2.5. Bronchoalveolar lavage fluid (BALF) analysis

Pups were sacrificed on P14, with 2 volumes of 300 μL of cold 1 × PBS were instilled, gently aspirated, and pooled, BALF was collected via cannulation of the trachea and lung lavage. Cells were prepared by cytocentrifugation, and stained with Geimsa. The total number of immune cells was counted using a Neubauer-improved and expressed per milliliter of BALF.

2.6. iNKT cells in lung tissue of newborn mice were detected by flow cytometry

To analyze iNKT cells in mouse lung tissues, we first collected lung tissues at P3, P7, P10, and P14 days after normoxia and hyperoxia exposure, filtered them through a 70 μm cell strainer, and stained with Fixable viability dye EF780 (eBioscience, USA) to distinguish viable cells. Finally, staining was performed with NK1.1-PE-Cy7, CD3-FITC, and CD69-PE antibodies (BioLegend, USA). CD3/NK1.1 double intermediate positive cells were defined as iNKT cells as previously described [34,35]. The activation status of iNKT cells was next assessed with CD69 [35].

2.7. iNKT cells were blocked or specific activation in mice

Newborn hyperoxia group mice were intraperitoneally injected with anti-CD1d neutralizing antibody (BioXCell, USA) to inhibit iNKT cells activation at P7(10 μg/g, once a day for 4 consecutive days, while mice in the control group were injected with IgG) [36]. To activate iNKT cells, mice were instilled with 2 μg α-Galcer (Aladdin, China) via nasal drip for 4 days [37]. Three days after the end of the intervention, which was 14 days after birth, lung tissue samples were collected. H&E staining was used to observe the pathological changes of the lung, PAS was used to observe the lung development, and the lung differentiation was evaluated by WB and immunofluorescence.

2.8. iNKT cells were sorted from mice lung tissue by magnetic beads

iNKT cells in normal C57BL/6 mouse lung tissues were extracted from mouse tissues using the mouse $NK1.1^+$ iNKT cell isolation kit (Miltenyi Biotec, Germany). iNKT cells were sorted by magnetic-activated cell sorting (MACS) system according to the manufacturer's instructions. Cell purity was detected by flow cytometry, purity greater than 95 % was used for subsequent experiments. The iNKT cells suspension was dropped on the slide, and the cell specimens on the slide were driven at a uniform speed to make cell smears. After natural drying, the slides were dropped with Wray-Giemsa composite staining solution (Solebo, China) for staining for 5 min, and buffer solution was added for staining for 5 min. After repeated washing, the slides were dried and fixed. Microscopic observation and photographs were taken by Leica microscope.

2.9. Adoptive transfer of lung tissue-derived iNKT cells

Extraction of iNKT cells from normal mouse lung tissue 1×10^6 cells/ml were resuspended in RPMI-1640 medium, counted and seeded in 6-well plates. DiR also known as Cy7 DiC18, was purchased from aladdin Biotech Co., LTD., in 2.5 mg/mL was dissolved in DMSO and stored at 4 °C, then DiR solution was diluted, added and incubated for half an hour at 37 °C, 5 % CO_2. After washing with PBS, the cells suspension was centrifuged at 500 g, 5 min at 4 °C, washed, resuspended, and injected into P10 mice in the normoxia and hyperoxia group by tail vein injection technique (5×10^5 cells/mouse). The fluorescence labeling of cells was observed using a small animal in vivo imaging system, and pictures were taken at 0, 30 min, 12 h and 24 h. At different time points, the small animal in vivo imaging system was used to detect the changes in migration of iNKT cells after adoptive transfer in mice. Finally, the mice were sacrificed, and heart, liver, spleen, lung, and kidney were harvested and imaged ex vivo. The effect of adoptive transfer of iNKT cells in mice on lung differentiation was also observed.

2.10. Cell culture and transwell AEC II-iNKT co-culture construction

The MLE12 cell line was purchased from Servicebio. MLE12 cells have characteristics of type II alveolar epithelium and are commonly used as AEC II in mice [38]. AEC II were cultured in DMEM/F12 medium with 10 % FBS at 37 °C in 5 % CO_2. AEC II-iNKT co-culture system: iNKT cells were seeded in 0.4 μm transwell chambers at the number of 1×10^4 cells/well, and AEC II were seeded uniformly in 24-well plates. After AEC II attachment, transwell inserts containing iNKT cells were moved into wells where AEC II was attached and incubated for 72 h under normoxia and hyperoxia conditions. In addition, AEC II was cultured under normoxia and hyperoxia alone for 72 h. In vitro, we used a hypoxia chamber device from billups-rothenberg Company. The treated well plate was placed into the middle layer and closed, the oxygen cylinder was connected, and the oxygen concentration was detected at the same time. The supernatant and lower layer were collected for subsequent detection.

2.11. RNA sequencing was performed on AEC II that were incubated with or without iNKT cells

After 72 h of AEC II-iNKT cells co-culture, total RNA was extracted from AEC II by trizol reagent (Absin, China), and transcriptome sequencing was performed to analyze the possible mechanism of iNKT cells affecting AEC II differentiation. RNA libraries were sequenced on Illumina sequencing platform (Gene Denovo Biotechnology, China). Raw gene expression levels were normalized to fragments per kilobase transcript per million mapped reads (FPKM). By filtering the edgeR gm benchmark ($|\log_2 fc| > 1.5$, $p < 0.05$) were applied to the FPKM values to identify differentially expressed genes (DEGs).

2.12. Fe^{2+}, IL-17A and IL-6 were detected by enzyme-linked immunosorbent assay (ELISA)

Different groups of cells were detected according to the instructions, the contents of Fe^{2+} (Solarbio, China), IL-17A (Lianke Biological, China) and IL-6 (Vazyme, China) were determined by ELISA.

2.13. Lipid peroxidation and malondialdehyde (MDA)

The C11 biodipy fluorescent probe was added into the supernatant of cell culture medium at a final concentration of 10 μM and incubated for 40 min to detect lipid peroxidation levels in AEC II. To assess the level of concentration in each group, the concentration of MDA in cell lysates was assessed using an MDA assay kit (Beyotime, China).

2.14. The protein levels of surfactant protein C (SP–C) and podoplanin (PDPN/T1α), ferroptosis-related markers glutathione peroxidase 4 (GPX4), ferritin heavy chain(FTH1) and prostaglandin endoperoxide synthase2(PTGS2) were detected by western blot (WB)

Different groups of cell or tissue lysates were extracted using RIPA lysis buffer (Beyotime, China) supplemented with protease inhibitor (NCM Biotech, China), total proteins were separated by SDS-PAGE and transferred to PVDF membranes (Millipore, USA). The cells were then treated with rapid blocking solution (NCM Biotech, China) for 10 min at room temperature. Blots were examined overnight at 4 °C with primary antibodies. Secondary antibodies (1:1000 dilution) conjugated to the HRP corresponding to the species were then introduced. Enhanced chemiluminescence reagents (ThermoFisher Scientific, USA) were used to visualize the protein bands. Primary antibodies anti-SP-C, anti-T1α, anti-GPX4, anti-PTGS2, anti-FTH1 and β-actin were purchased from Abcam, Proteintech, Wanleibio and Santa Cruz. The goat anti-rabbit/mouse IgG H&L (HRP)(secondary antibody) were purchased from Beyotime.

2.15. The expression of SP-C and T1α in lung tissue and cells were detected by

immunofluorescence

After paraffin block sectioning, deparaffinization, xylene treatment and alcohol gradient dehydration, antigen repair was performed in sodium citrate buffer (Biosharp, China), the lung tissue was marked with a histochemical pen (Biosharp, China). Cells needed to be seeded in well plates with cell slides (Biosharp, China), and the supernatant was uniformly discarded at the end point of collection, fixed with 4 % paraformaldehyde for 15 min, and washed with PBS. For tissue and cellular immunofluorescence, the blocking solution prepared by mixing BSA and Triton was added, placed at 4 °C for 30 min, rinsed with PBS, and diluted immunofluorescence antibody was added according to the instructions of the antibody anti-SP-C and anti-T1α. The secondary immunofluorescent antibody (Abcam, USA) was diluted with the dilution of immunofluorescent secondary antibody (Beyotime, China), and then placed at room temperature in a dark place for 1.5 h. After washing, DAPI Fluoromount-G® (SouthernBiotech, USA) was added, and the cells were observed and filmed under a Thunder fluorescence microscope (Leica, Japan). The number of AEC II/AEC I positive cells were determined by analyzing the fluorescence intensity of SP-C/T1α using image software. Image J software was used to analyze the co-localization of SP-C/T1α positive cells.

2.16. The ferroptosis-related markers GPX4, FTH1 and PTGS2 were detected by quantitative real-time PCR (qRT-PCR)

Total RNA was extracted by RNA Rapid purification kit (YiShan Biotechnology, China). cDNA was synthesized by PrimeScript RT Master Mix (TaKaRa, Japan). qRT-PCR was performed using SYBR Green qPCR kit (Vazyme, China). Relative gene expression was identified using the $2^{-\Delta\Delta Ct}$ method and normalized to β-actin. The primers were synthesized by Sangon Biotech.

2.17. AEC II morphology was observed by transmission electron microscope

The AEC II of different groups were collected, the medium was discarded, fixed in electron microscope fixative(2.5 % glutaraldehyde), and the cell suspension was centrifuged into clusters. The ultrastructural changes of ferroptosis in AEC II were observed by transmission electron microscopy (Hitachi, Japan), which was performed by Servicebio Biotechnology.

2.18. Effect of ferroptosis on AEC II on the expression of SP-C and T1α

To investigate the effect of ferroptosis on the expression of SP-C and T1α under hyperoxia, 1 μM ferroptosis agonists Erastin (MCE, USA) and 0.1 μM ferroptosis inhibitor ferrostein-1(Fer-1, MCE, USA) were added respectively, then were divided into six groups: Hyperoxia + DMSO, Hyperoxia + iNKT cells + DMSO, Hyperoxia + Erastin, Hyperoxia + iNKT cells + Erastin, Hyperoxia + Fer-1, and Hyperoxia + iNKT cells + Fer-1, and the differentiation of

AEC II were detected by WB.

2.19. Statistics

GraphPad Prism 9.0 was used for statistical analysis. Inter-group variables were compared using Student's *t*-test or one-way analysis of variance (ANOVA). All experiments were repeated at least three times. All results were represented by mean ± standard deviation (SD), and statistical significance was determined by a *p* value of less than 0.05 ($*P<0.05$, $**P<0.01$, $***P<0.001$).

3. Results

3.1. Activation of NKT cells in peripheral blood of patients with BPD

Since IL-15 is a major cytokine responsible for the development, maturation, and survival of NKT cells [26], we downloaded GEO data GSE32472 to explore IL-15 mRNA levels in peripheral blood on days 5 and 14 with BPD progression. The expression of IL-15 gradually increased with the progression of BPD (Fig. 1A). We first aimed to determine the percentage of NKT cells ($CD45^+CD56^+CD3^+$) in peripheral blood (Fig. 1B). Patients with BPD had an increased percentage of NKT cells (Fig. 1C and D) and the △MFI of the activation markers CD69 relative to isotype controls was analyzed on NKT cells ($CD3^+CD56^+$) in BPD group and non-BPD group (Fig. 1E). These results suggest that: NKT cells may be involved in the pathological process of BPD.

Fig. 1.

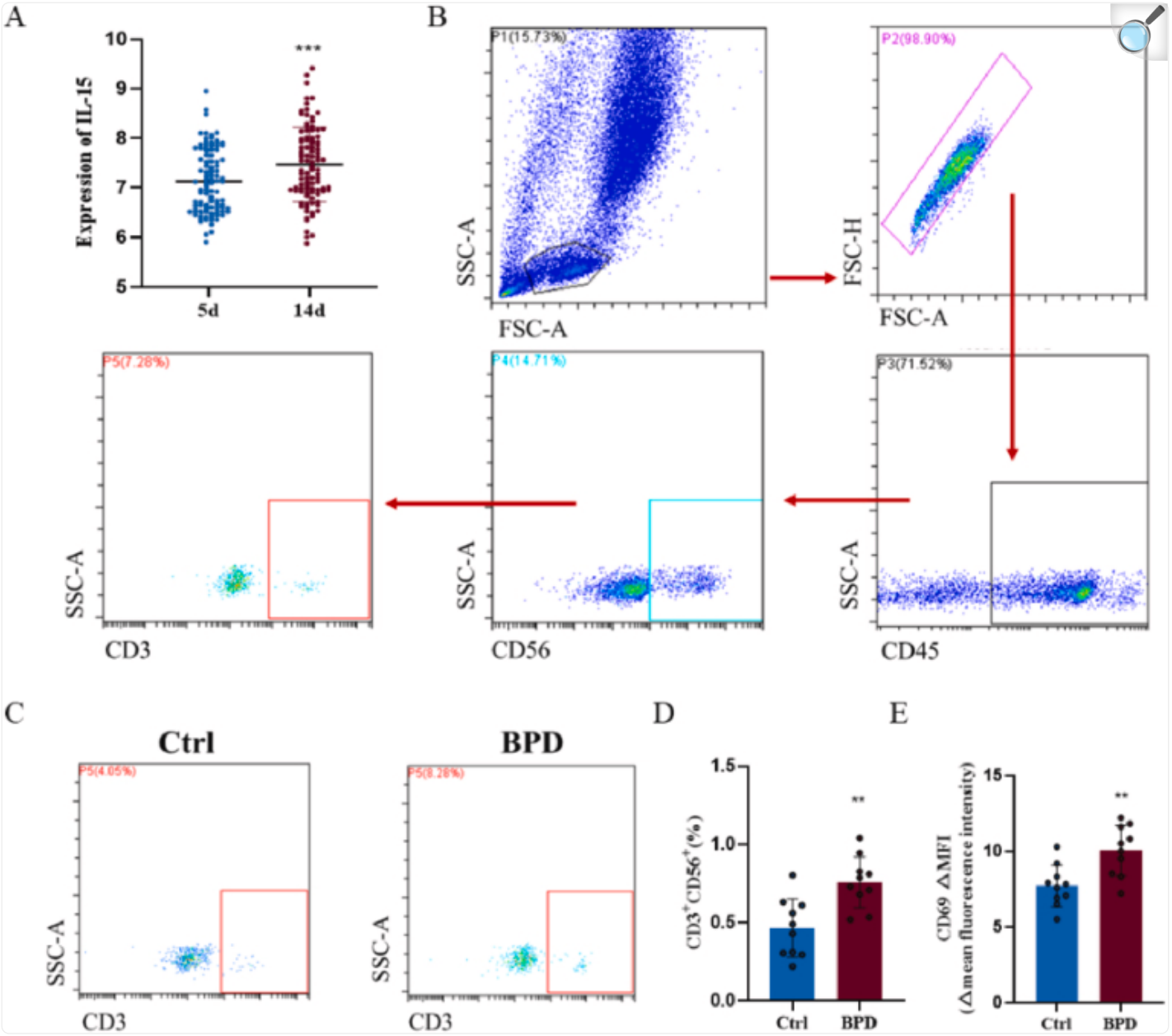

Open in a new tab

Characteristics of NKT cells in the blood of healthy controls and patients with BPD

A. Analysis of peripheral blood IL-15 expression in the dataset. B. Representative FACS analysis showing the gating strategy used to identify $CD45^{+}$ $CD56^{+}CD3^{+}$NKT cells in the peripheral blood. C. Representative results of NKT cells detected by flow cytometry in the peripheral blood of healthy controls and patients with BPD. D. Percentage of NKT cells detected by flow cytometry in the peripheral blood of ten healthy controls

and ten patients with BPD. E. CD69 MFI of activation marker of NKT cells relative to isotype controls. (* * $P<0.01$, * * * $P<0.001$).

3.2. BPD mice were constructed, and there were disorders of lung development

In this study, we constructed a mouse model of BPD induced by hyperoxia. The body size changes of mice under normoxia and hyperoxia at P3, P7, P10, and P14 were evaluated and compared. The body size development of hyperoxia group was lagging behind that of mice grown in normoxia group (Fig. 2A, Supplementary Fig. 1A). Relative to the normoxia group, the number of immune cells in BALF increased in hyperoxia group at P14 (Fig. 2B). To evaluate the pathological changes in lung tissue by H&E staining was used. Hyperoxia group mice had disordered alveolar structure with progressive thickening of alveolar walls, decreased number of alveoli, and simplified structure, lung volume decreased, RAC decreased, and MLI increased, (Fig. 2C–E). To assess lung development, we used PAS staining to detect glycogen in lung epithelial cells.We used tissue immunofluorescence and WB for the SP-C (AEC II-specific marker) and T1α (AEC I-specific marker). In the present study, pulmonary epithelial glycogen content was measured by PAS staining, the epithelial content of glycogen reflects the development and maturation of the lung [39], and it was found that hyperoxia group mice had increased glycogen content compared with normoxia group mice at P14 (Fig. 2F). Immunofluorescence double staining showed that the expression of both SP-C and T1α was decreased, and the number of $T1\alpha^{+}$ $SP\text{-}C^{+}$ cells (% total $SP\text{-}C^{+}$ cells) was decreased (Fig. 2G). WB results showed that the protein expressions of SP-C and T1α in lung tissue of hyperoxia group mice were lower than those of the normoxia group (Fig. 2H).

Fig. 2.

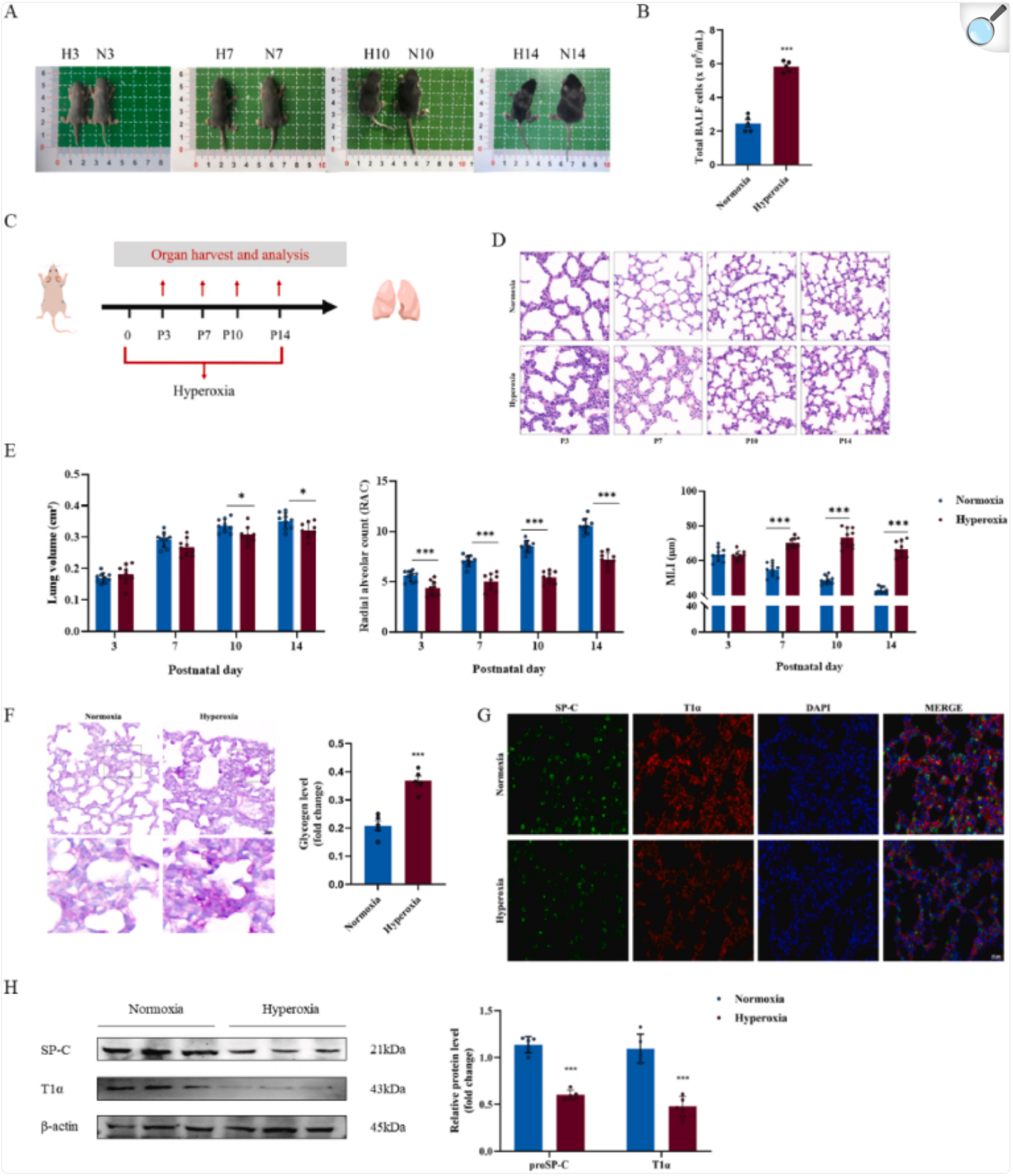

Open in a new tab

BPD mice were constructed, and there were disorders of lung development

A. Mouse pups were exposed to normoxia (21 % O_2) or hyperoxia (85 % O_2) from the day of birth. The body size of normoxia and hyperoxia groups of mice at P3, P7, P10, and P14 was compared. H, hyperoxia; N, normoxia. B. The total number of immune cells in BALF in normoxia and hyperoxia groups of mice at P14. n = 5/group. C. Lung tissues were obtained at P3, P7, P10, and P14. D. Representative tissue sections of lungs by H&E at 21 % O_2 or 85 % O_2 at P3, P7, P10, and P14. n = 9/group. Scale bar = 50 μm. E. Assessment of lung volume according to Archimedes' principle. Lung morphometry was quantified by RAC and MLI measurements. F. PAS staining was used to evaluate and compare the degree of development between normoxia and hyperoxia at P14. n = 5/group. Scale bar = 50 μm. G. Immunofluorescence detection of SP-C and T1α in lungs of the normoxia and hyperoxia groups lung tissue at P14. n = 5/group. Scale bar = 50 μm. H.WB measured and quantified the protein levels of SP-C and T1α in lungs of the normoxia and hyperoxia groups at P14. n = 5/group. ($*P<0.05$, $***P<0.001$).

3.3. Hyperoxia exposure promoted the accumulation and activation of iNKT cells in the lungs of mice

The recruitment of $CD45^+$ immune cells after hyperoxia exposure was increased (+20 %–30 %) compared with the normal group at P14 (Supplementary Fig. 1B). The percentage of iNKT cells in the lung increased after hyperoxia exposure (Fig. 3A–C). Meanwhile, the expression of CD69 (a marker of iNKT cells activation) on iNKT cells was continuously increased in hyperoxia group at P7 by flow cytometry (Fig. 3D). Hyperoxia exposure resulted in increased recruitment or a local expansion of activated iNKT cells in the lungs.

Fig. 3.

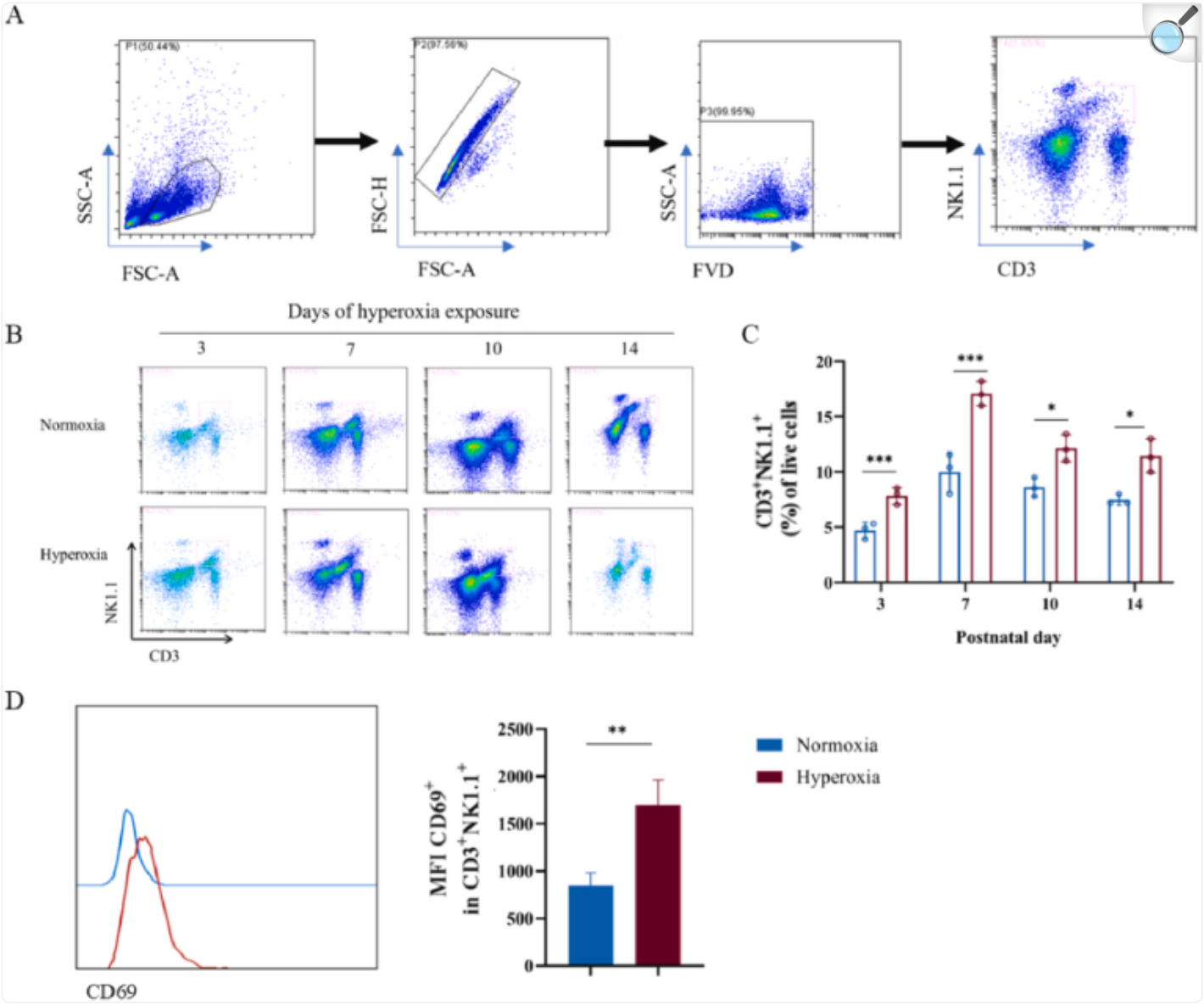

Open in a new tab

Hyperoxia exposure increased the number of iNKT cells in the lung and triggered their activation

A. Representative FACS analysis showing the gating strategy used to identify FVD$^-$ CD3$^+$NK1.1$^+$iNKT cells at P3, P7, P10, and P14 in normoxia and hyperoxia groups. B. Representative results of iNKT cells in the lungs of normoxia and hyperoxia groups at P3, P7, P10, and P14. C. Percentage of iNKT cells in the lungs of normoxia and hyperoxia groups at P3, P7, P10, and P14. n = 3/group. D. CD69 MFI of iNKT cells in normoxia and hyperoxia groups at P7. (* $P<0.05$, * * $P<0.01$, * * * $P<0.001$).

3.4. Inhibition of iNKT cells activation alleviated abnormal lung development in BPD mice

To determine whether iNKT cells contributed to the observed lung injury, hyperoxia mice were treated with anti-CD1d antibody (or isotype control antibody) to limit iNKT cells activation and reduce their numbers [36]. Treatment of mice in the hyperoxia group with anti-CD1d significantly reduced cell numbers in the BALF compared with the use of anti-IgG controls (Fig. 4A). Hyperoxia group mice were intraperitoneally injected with anti-CD1d antibody to inhibit iNKT cells activation and abundance, the alveolar structure tends to be regular, the number of alveoli increases, and the alveolar walls become thinner, RAC increased and MLI decreased (Fig. 4B–C). The glycogen content of the contrast lung epithelium was evaluated and decreased after administration of anti-CD1d in hyperoxia group by PAS staining (Fig. 4B–C). The results of immunofluorescence double staining showed that the expression of SP-C and T1α in lung tissues of hyperoxia group mice treated with anti-CD1d neutralizing antibody was increased at P14, and $T1\alpha^{+}$ $SP\text{-}C^{+}$ cells (% total $SP\text{-}C^{+}$ cells) were increased compared with hyperoxia group mice (Fig. 4D). WB results showed that the protein expression of SP-C and T1α in the lung tissue of the hyperoxia group was decreased, and SP-C and T1α were increased in hyperoxia group mice treated with anti-CD1d (Fig. 4E).

Fig. 4.

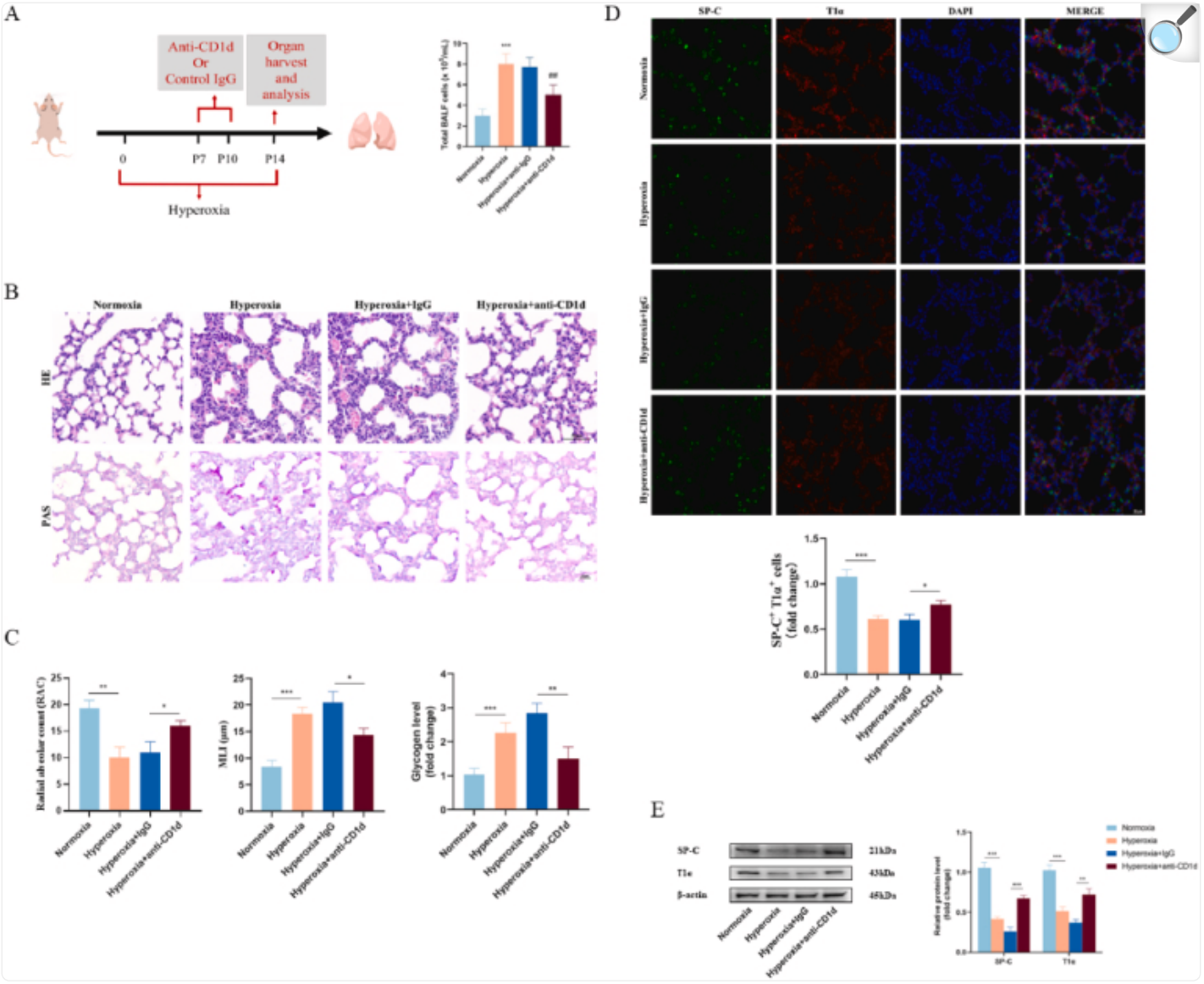

Open in a new tab

Inhibition of iNKT cells activation alleviates abnormal lung development in BPD mice

A. Mouse pups were exposed to either room air (21 % O_2) or hyperoxia (85 % O_2) from the day of birth. anti-CD1d or control IgG were injected at P7-10, BALF analysis and lung tissues were harvested at P14. n = 5/group. B. H&E and PAS show the presentative tissue sections of lungs under different treatment conditions at P14. Scale bar = 50 μm. C. Lung morphometry was quantified by RAC and MLI measurements. Statistical plot of PAS staining to assess the extent of development under different treatments at P14. n = 5/group. D. Comparison of immunofluorescence detection of SP-C and T1α in lung tissues under normoxia group,

hyperoxia group, hyperoxia group injected control IgG and hyperoxia group injected anti-CD1d conditions at P14. The proportion of T1α^{+} SP-C^{+} cells (% total SP-C^{+} cells) in immunofluorescence staining was quantified. Scale bar = 50 μm. E. WB was used to detect the protein levels of SP-C and T1α in lung tissue of different groups at P14. Quantitative analysis of WB detection levels. ($*P<0.05$, $**P<0.01$, $***P<0.001$).

3.5. Specific activation of iNKT cells and increased number of iNKT cells aggravated lung disorders in BPD mice

To understand the role of pulmonary iNKT cells in the pathogenesis of BPD, mice were given α-GalCer intranasal at P7 for 4 days and examined the features of BPD pathology at P14 (Fig. 5A). Repeated intranasal administration of α-GalCer to mice showed no abnormal appearance or behavior. α-GalCer significantly increased the number of iNKT cells detected by flow cytometry and the gene expression marker Vα14Jα18 in the lung (Supplementary Figs. 1C–D). As shown in Fig. 5B, observed in hyperoxia group mice with repeated administration of α-GalCer, H&E showed enlarged alveoli and marked cellular infiltrates in the lungs of mice given repeated α-GalCer, which were not found in the lungs of treated control IgG. The degree of impairment in lung parameters was increased compared with hyperoxia group mice, specifically, RAC decreased and MLI increased (Fig. 5B–C). The proinflammatory cytokines IL-6 and IL-17A were increased in the lungs of mice treated with α-GalCer compared with mice treated with control (Supplementary Figs. 1E–F). The epithelial content of contrast glycogen was evaluated, and glycogen staining increased after α-GalCer administration compared with hyperoxia group mice (Fig. 5B–C). To further verify the effect of the number and activation of iNKT cells on BPD mice, iNKT cells in the lungs of mice were sorted by magnetic beads, and their purity was identified by flow cytometry, its purity was more than 95 % (Supplementary Fig. 1G). After adoptive transfer of iNKT cells via tail vein, they were placed in the normoxia and hyperoxia environment respectively. DiR-labeled iNKT cells were detected by in vivo small animal imaging at the time of adoptive transfusion, 30 min, 12 h and 24 h. The iNKT cells were mainly concentrated in the liver and lung. Compared with the normoxia group, the hyperoxia group had stronger fluorescence intensity of DiR stained iNKT cells in vivo, and significantly increased fluorescence intensity in liver and lung, suggesting that hyperoxia could induce recruitment of iNKT cells in lung (Fig. 5D). At the same time, after adoptive transfer of iNKT cells to the hyperoxia group at P10, showed disordered alveolar structure, larger alveolar fusion, reduced number, simplified structure, thickened alveolar wall, and increased inflammatory cells compared with the control group at P14 (Fig. 5G–H). WB results showed that SP-C and T1α protein expression in the lung tissue of the hyperoxia group was decreased, and SP-C and T1α protein expression was significantly decreased in hyperoxia group mice adoptive transfer with iNKT cells (Fig. 5F). The results of immunofluorescence double staining showed that the expression of SP-C and T1α in the lung tissue of hyperoxia group mice adoptive transfer with iNKT cells detected at P14 was decreased, and T1α^{+}SP-C^{+} cells (% total SP-C^{+} cells) were decreased compared with hyperoxia group mice (Fig. 5E). These results indicate that the pathological manifestations of BPD are aggravated after the use of iNKT cells-specific activators and adoptive transfer of iNKT cells.

Fig. 5.

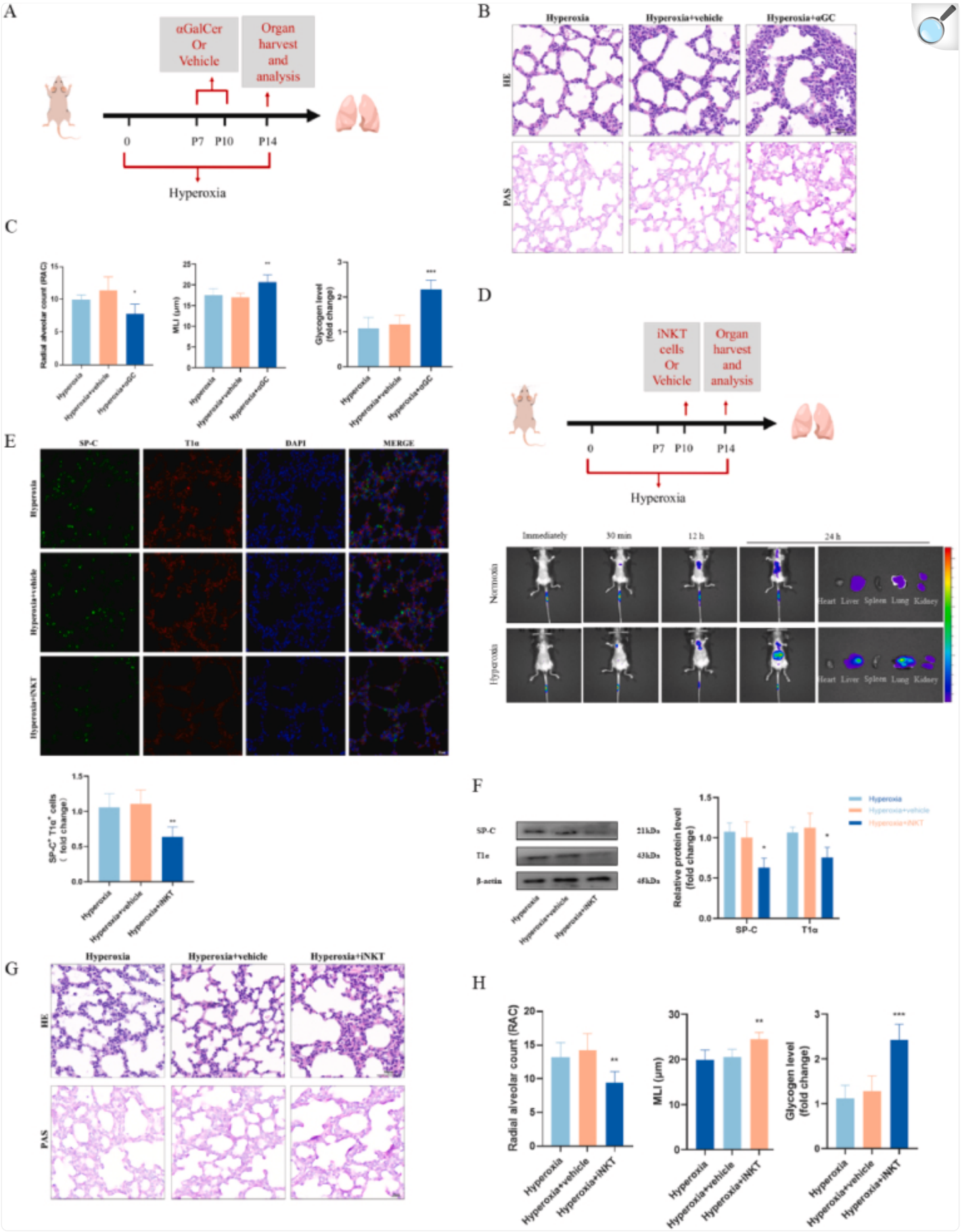

Open in a new tab

Specific activation of iNKT cells and increased number of iNKT cells aggravate lung disorder in BPD mice

A. Mouse pups were exposed to normoxia (21 % O_2) or hyperoxia (85 % O_2) from the day of birth. α-GalCer or vehicle were used at P7-10, and lung tissues were harvested at P14. n = 5/group. B. H&E and PAS show the presentative tissue sections of lungs under different treatment conditions at P14. n = 5/group. Scale bar = 50 μm. C. Lung morphometry was quantified by RAC and MLI measurements. Statistical plot of glycogen staining to assess the extent of development under different treatments at P14. D. Schematic representation of adoptive transfer of iNKT cells at P10. n = 5/group. iNKT cells was imaged in vivo at 0, 30 min, 12 h and 24 h after adoptive transfer in normoxia group and hyperoxia group mice. E. Comparison of immunofluorescence detection of SP-C and T1α in lung tissues of hyperoxia group, hyperoxia group injected vehicle and hyperoxia group adoptive transfer iNKT cells conditions at P14. The proportion of $T1\alpha^+$ $SP\text{-}C^+$ cells (% total $SP\text{-}C^+$ cells) in IF staining was quantified. n = 5/group. Scale bar = 50 μm. F. WB was used to detect the protein levels of SP-C and T1α at P14. Quantitative analysis of WB detection levels. G. H&E and PAS show the presentative tissue sections of lungs under different treatment conditions at P14. Scale bar = 50 μm. H. Lung morphometry was quantified by RAC and MLI measurements. Statistical plot of PAS staining to assess the extent of development under different treatments at P14. n = 5/group. ($*$ $P<0.05$, $**$ $P<0.01$, $***$ $P<0.001$).

3.6. AEC II-iNKT cells co-culture and the effect of iNKT cells on AEC II under hyperoxia

To investigate the effect of iNKT cells on AEC II, we established AEC II-iNKT cells transwell co-culture model under normoxia and hyperoxia, respectively. iNKT cells were sorted by magnetic beads and stained by Wright-Giemsa staining. The cells were round in shape, consistent with the characteristics of lymphocytes (Fig. 6A). AEC II was cultured alone or with iNKT cells sorted by magnetic beads and exposed to normoxia and hyperoxia for 72 h, respectively (Fig. 6B). WB was used to detect the expression of SP-C and T1α in AEC II, after 72 h of exposure in compared with the normoxia group, the expression of SP-C in AEC II in hyperoxia group was significantly decreased, the expression level of T1α was increased. The expression of SP-C and T1α in AEC II + iNKT group was lower than the AEC II group under hyperoxia (Fig. 6C). Therefore, we performed immunofluorescence staining showed that the expression of SP-C was dominant in AEC II in normoxia group. However, the expression of SP-C was extremely low in hyperoxia group. SP-C and T1α were reduced, and colocalization was reduced in the AEC II + iNKT group compared with AEC II alone under hyperoxia (Fig. 6D). ELISA was used to detect increased IL-6 and IL-17A in the supernatant of iNKT cells co-cultured with AEC II (Supplementary Figs. 1H–I).

Fig. 6.

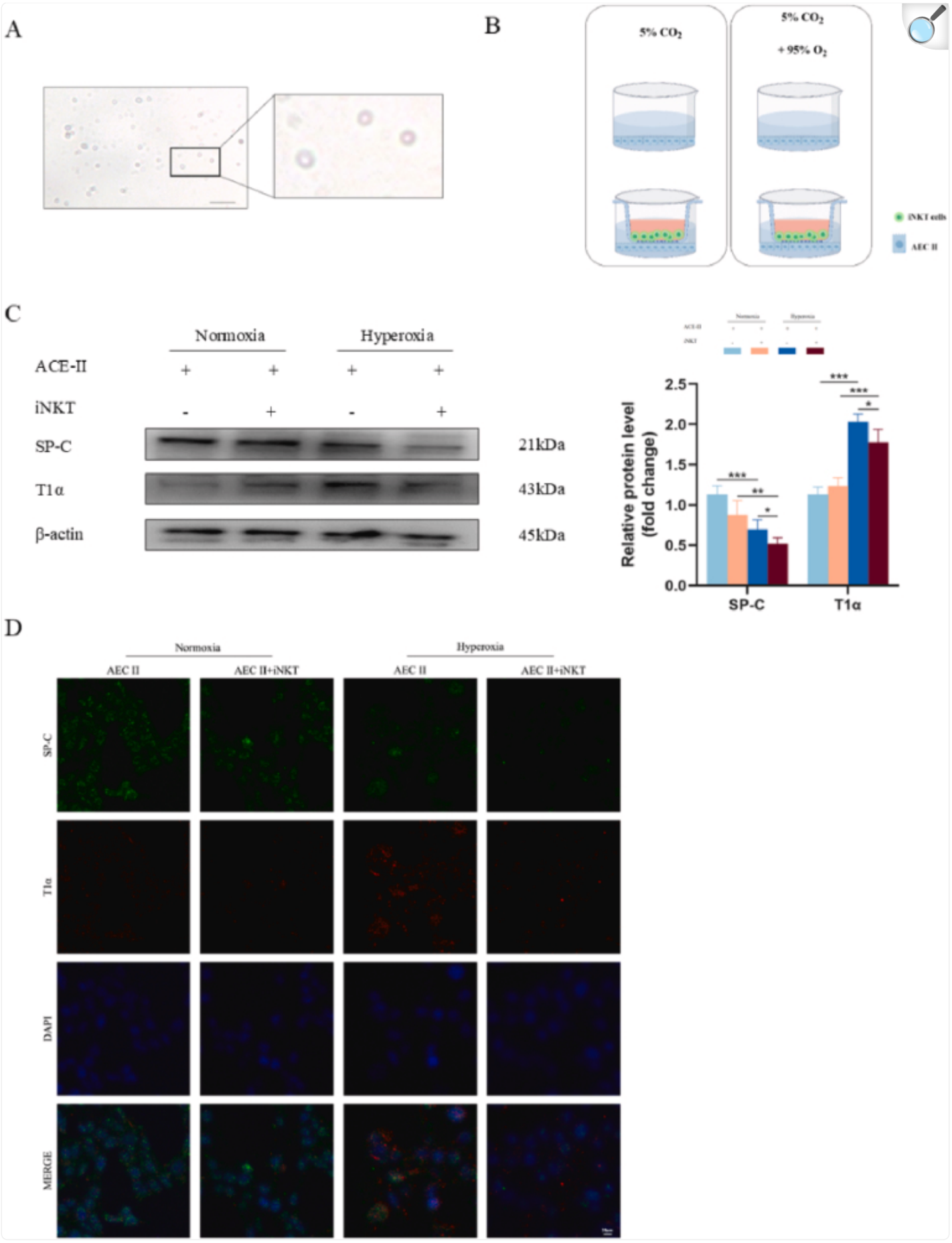

Open in a new tab

AEC II- iNKT cells co-culture and the effect of iNKT cells on AEC II under hyperoxia 72 h

A. Giemsa staining showed the morphological characteristics of iNKT cells sorted by magnetic beads. B. Schematic representation of cell grouping and treatment. C. WB analysis of SP-C, T1α protein levels. β-Actin was used as a load Control. D. AEC II immunofluorescence staining. Red fluorescence-labeled T1α, green fluorescence-labeled SP-C, and double-stained cells indicate cells in transdifferentiated state. Scale bar = 20 μm. ($*P<0.05$, $**P<0.01$, $***P<0.001$).

3.7. iNKT cells promote AEC II ferroptosis under hyperoxia

To further explore how iNKT cells contributes to AEC II under hyperoxia, the AEC II and AEC II + iNKT groups were cultured under hyperoxia for 72 h, and the extracted total RNA was subjected to RNA sequencing. $P<0.05$ and | log2fc |>1.5 genes were considered differentially expressed. Based on these, we find differentially expressed genes with programmed cell death in the GO database (http://www.geneontology.org/) related genes are compared, and ferroptosis was found the number of differentially expressed genes related to the highest in all genes associated with programmed cell death (Fig. 7A–B). Compared with AEC II under hyperoxia alone, the mRNA levels of GPX4 and FTH1 were significantly decreased and PTGS2 were increased in AEC II co-cultured with iNKT cells under hyperoxia (Fig. 7C). In addition, WB showed a significant decrease in GPX4 and FTH1 levels and an increase in PTGS2 (Fig. 7D). Lipid peroxidation was significantly increased as detected by C11 bodipy staining (Fig. 7E). Hyperoxia led to increased Fe^{2+} and MDA levels in AEC II, which increased when co-cultured with iNKT cells compared with AEC II alone group (Fig. 7F–G).

Fig. 7.

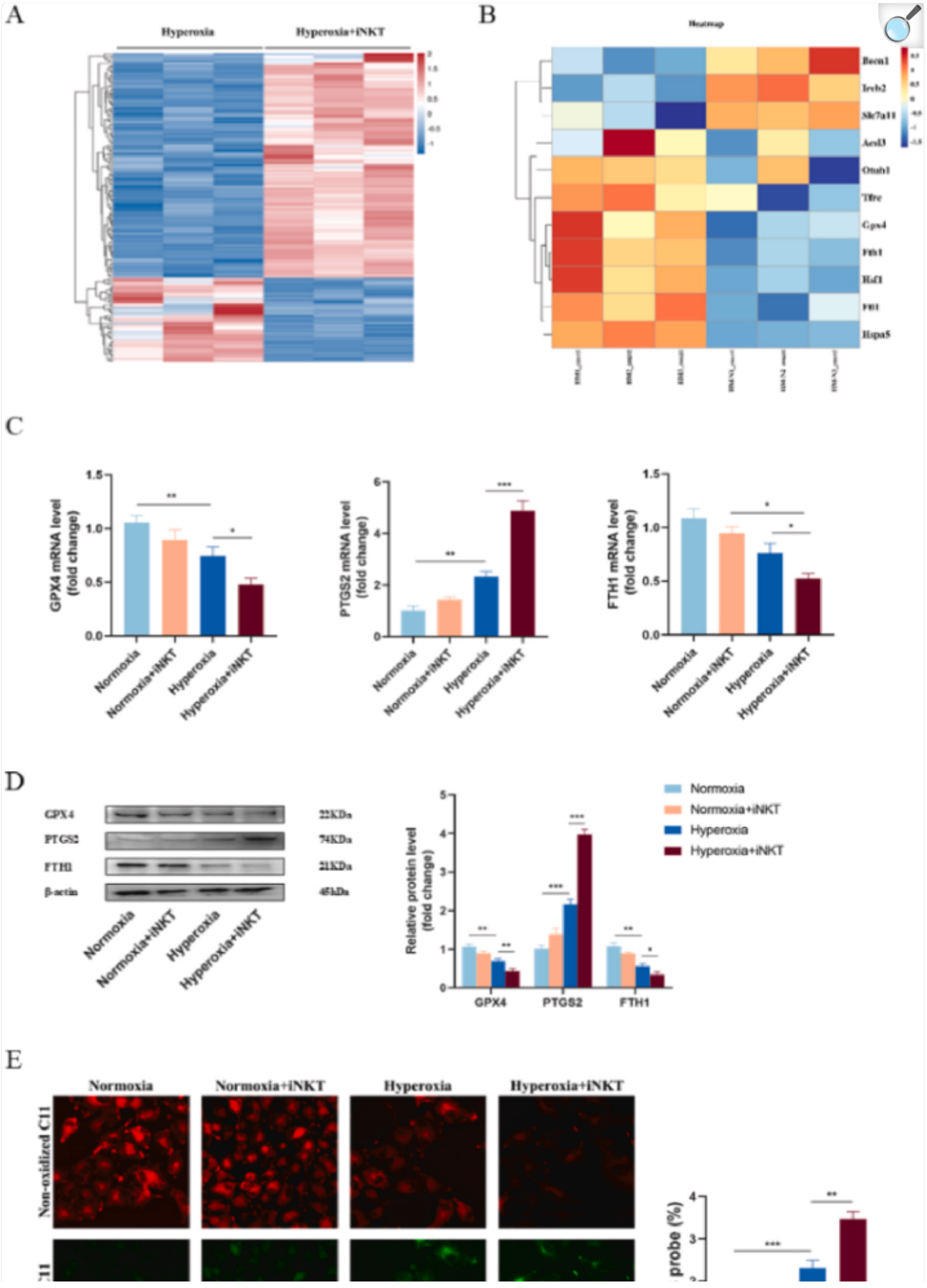
A
Hyperoxia
Hyperoxia+iNKT
B
Heatmap
Becn1
Ireb2
Slc7a11
Acsl3
Otub1
Tfrc
Gpx4
Fth1
Hif1
Ftl1
Hspa5
C
GPX4 mRNA level (fold change)
PTGS2 mRNA level (fold change)
FTH1 mRNA level (fold change)
Normoxia
Normoxia+iNKT
Hyperoxia
Hyperoxia+iNKT
D
GPX4
PTGS2
FTH1
β-actin
22KDa
74KDa
21KDa
45kDa
Relative protein level (fold change)
E
Normoxia
Normoxia+iNKT
Hyperoxia
Hyperoxia+iNKT
Non-oxidized C11

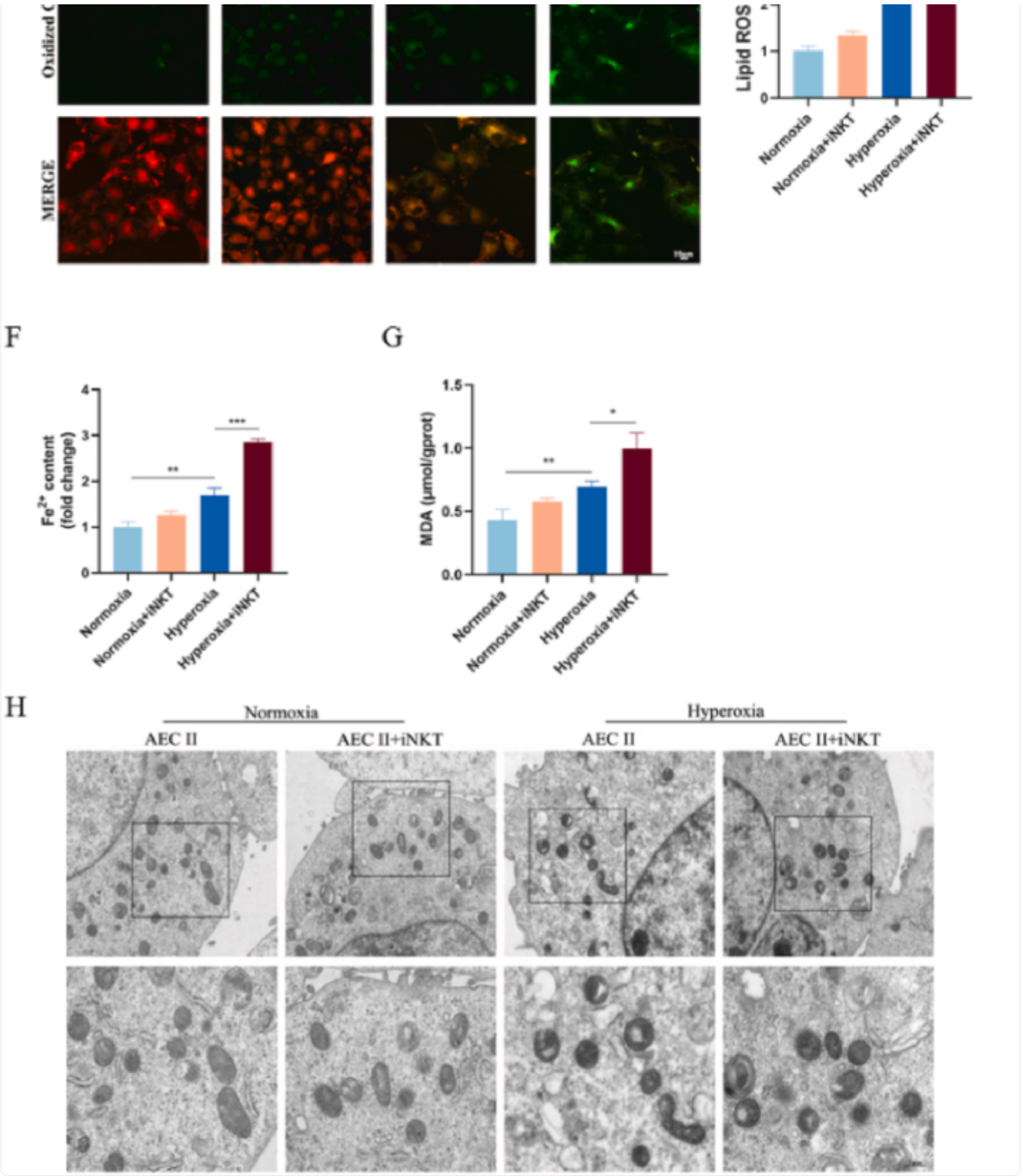

Open in a new tab

iNKT cells promote AEC II ferroptosis under hyperoxia

A Heat map shows the difference in gene expression between AEC II and AEC II + iNKT cells groups. B. Heat map depicting differential expression of ferroptosis-related genes. C. The mRNA expressions of GPX4,

FTH1 and PTGS2 were detected by qRT-PCR. D. The protein expressions of GPX4, FTH1 and PTGS2 were detected by WB. E. Lipid peroxidation levels were measured by C11 bodipy staining. F. The contents of Fe^{2+} in the epithelium were determined by ELISA. G. The concentration of MDA in cell lysates. H. Cell morphology was observed by transmission electron microscope. scale bar = 1 μm. (* $P<0.05$, * * $P<0.01$, * * * $P<0.001$).

Fig. 7H showed the characteristics of ferroptosis by transmission electron microscope (TEM), suggested that after under hyperoxia, the AEC II showed that decrease the size of the mitochondria membrane density increase, mitochondrial cristae decreased, mitochondrial outer membrane rupture, after AEC II-iNKT cells co-cultured under hyperoxia, the mitochondrial changes were even more pronounced. These results suggest that AEC II ferroptosis in hyperoxia may be associated with iNKT cells.

3.8. AEC II ferroptosis accompanied by decreased expression of SP-C and T1α

AEC II culture alone under hyperoxia, we found that after added the ferroptosis activator Erastin, GPX4 was decreased, PTGS2 was elevated, and SP-C and T1α were decreased compared to the AEC II + DMSO group under hyperoxia, and when the ferroptosis inhibitor Fer-1 was added, GPX4 was elevated, PTGS2 was decreased, and SP-C and T1α were elevated compared to the AEC II + DMSO group under hyperoxia. In AEC II + iNKT cells group under hyperoxia, after added the ferroptosis activator Erastin, we found that GPX4 was decreased, PTGS2 was increased, and T1α and SP-C were decreased compared with AEC II + iNKT cells + DMSO group. In AEC II-iNKT cells co-cultured system under hyperoxia, after add ferroptosis inhibitor Fer-1, showed that GPX4 was increased, PTGS2 was decreased, and T1α and SP-C were increased compared with AEC II + iNKT cells + DMSO group (Fig. 8A–B).

Fig. 8.

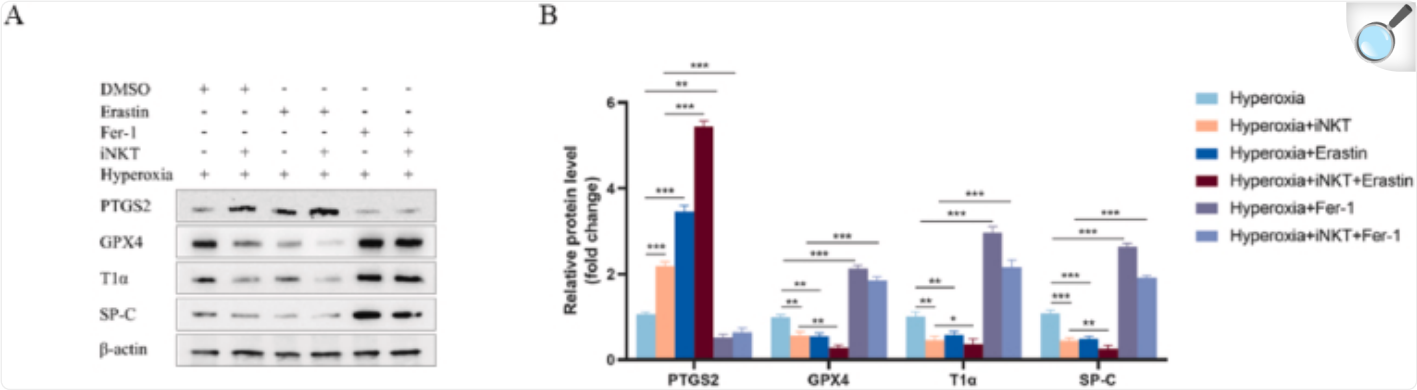

Open in a new tab

Ferroptosis relates to decreased SP-C and T1α

A-B. The protein expressions of PTGS2,GPX4, T1α, SP-C in each group were detected by WB. (* * $P<$ 0.01, * * * $P<0.001$).

4. Discussion

BPD is a common chronic lung disease in young preterm infants, and the main pathological change is alveolar dysfunction [40]. In our study, a classic neonatal mice model of BPD exposed to hyperoxia was used, H&E results showed that compared with the normoxia group, the hyperoxia group had simplified alveolar structure, reduced alveolar number, dilated alveolar space, and significantly thickened alveolar wall, this indicates that we have successfully established a mice model of BPD. At present, it is believed that AEC II injury is the key to lung epithelial injury and is the pathological basis of BPD [41]. AEC II is the main stem cell in the lung, which can differentiate into AEC I to maintain lung homeostasis. In the recent study, AEC II was labeled with SP-C and E-cadherin, and differentiation of AEC II was evaluated by qRT-PCR and immunostaining/western blot [42]. SP-C is a highly specific AEC II cell marker. T1α is AEC I cell marker. Differentiated AEC II and AEC I cells differ phenotypically and express different cell-specific marker. SP-C^+/T1α^+ cells refer to the co-expression situation of these two markers, suggesting that these cells may be in a transformed or partially differentiated state. Certainly, the expression of SP-C^+/T1α^+ may also be heterogeneous during the differentiation of AEC II into AEC I, this was also initially confirmed in previous study [43], however, SP-C^+/T1α^+ double labeling of AEC II can be used to determine the differentiation of AEC II into AEC I. We found that the proportion of SP-C and T1α double-stained cells was significantly lower in the hyperoxia group

compared with the normoxia group, and a decrease in SP-C expression without a corresponding increase in T1α expression under hyperoxia by WB analysis of lung tissue. Glycogen is an important substance that reflects the maturity of ACE II [44]. With cell differentiation, glycogen is consumed and converted into alveolar surfactant phospholipids, so PAS staining can be used to assess pulmonary differentiation, we also found glycogen content was increased in the hyperoxia group compared with the normoxia group of littermates, these results suggested that hyperoxia reduced SP-C and T1α, and may related to abnormal AEC II differentiation.

Recent studies have found that changes of iNKT cells in the number and function play an important role in lung diseases. Under normal physiological conditions, iNKT cells are most abundant in the liver, spleen and lung, when in inflammation or infection, such as in pulmonary asthma [45], acute hyperoxic lung injury [46], LPS-induced acute lung injury [47], COPD [21], ARDS [22] and sterile inflammation [48], iNKT cells can be significantly increased and activated in the lung to a certain extent, which is pathogenic. At present, the role of NKT in BPD is not clear. IL-15 is a developmental factor of NKT cells [26]. Microarray data analysis shows that BPD patients have a significant increase in IL-15, but it is not clear whether NKT cells activated and increased in BPD. Firstly, we examined the NKT cells in the peripheral blood of patients with BPD and found that NKT cells increased and activated in peripheral blood of patients with BPD, suggest that NKT cells may play a role in the development of BPD, but further studies are needed. So, we used hyperoxia to replicate the BPD model, and found that compared with the normoxia group, the percentage of iNKT cells in lung tissue was increased, and the CD69 representing their activation status was significantly increased, suggesting that NKT cells may be involved in the pathophysiological process of BPD. Studies suggested that iNKT cells activation is a key upstream event that promotes chronic inflammation and fibrosis, and it is involved in the type 1, type 2, and type 3 cytokine pathways to promote fibrosis [14]. iNKT cells activation has also been shown to play a key role in promoting Wnt signaling and promoting the transition of epithelial cells to myofibroblasts [15]. To further investigate whether the increase and activation of iNKT cells is associated with impaired lung differentiation in BPD, we used anti-CD1d neutralizing antibody interfering with iNKT cells activation status in BPD mice, the number of immune cells in BALF significantly reduced, H&E staining showed that as the activation status and abundance of iNKT cells decreased, the alveolar structure tended to be regular, the number of alveoli increased and alveoli cavity was more uniform, RAC increased and MLI decreased, PAS showed a decrease in glycogen, WB and tissue immunofluorescence showed that SP-C, T1α increased, and fluorescence localization showed that SP-C and T1α co-localization increased, these results suggested that the abnormal development in BPD mice was alleviated after using anti-CD1d neutralizing antibody. It has been shown that treatment with anti-human CD1d antibody in a primate inflammation model, significantly reduces the number of macrophages, lymphocytes, eosinophils, and basophils in BALF. Previous studies have found that partial inhibition of iNKT cells activation by anti-CD1d antibody can reduce the release of cytokines in septic mice, thereby reducing the damage of organ function and ultimately reducing the mortality of septic mice [49]. Treatment of ischemia-reperfusion injury model mice with anti-CD1d antibody alleviated lung dysfunction and inflammation [36], important features of COPD, such as inflammation and emphysema, were significantly suppressed in $CD1d^{-/-}$ lacking iNKT cells [21], CD1d deficiency has a protective effect on FA-induced renal fibrosis in mice [50,51]. The above studies suggest that blocking iNKT cell activation reduces alveolarization disorders in BPD and may be related to promoting lung

differentiation.

To further investigate whether iNKT cells activation exacerbates lung development disorder in BPD, in this study, we used nasal instillation of α-Galcer, a specific activator of iNKT cells [29], in addition to extract iNKT cells by magnetic beads and adoptive transfer into mice via the tail vein. We found that BPD mice treated with α-GalCer showed more disordered alveolar structure, larger alveolar fusion, reduced number, simplified structure, thickened alveolar wall, and increased inflammatory cells by H&E. PAS staining showed increased glycogen accumulation. We successfully sorted iNKT cells with a purity greater than 95 %, and after adoptive transfer into BPD mice, iNKT cells reached the lungs after 30 min of in vivo imaging observation. In a similar study to adoptive transfer, iNKT cells were found to first reach the lungs within 15 min [52]. Next, after successful adoptive transfer of iNKT cells, mice were exposed to hyperoxia for 4 days, and lung tissues were collected at P14. We found recruitment of iNKT cells in the lungs of the hyperoxia group, accompanied by an increase in glycogen by PAS staining, decreased expression of SP-C and T1α by WB and decreased co-localization of SP-C and T1α by immunofluorescence, these results showed that the lung disorder of BPD mice was aggravated after adoptive transfer iNKT cells. It has been suggested that repeated use of αGalCer to activate pulmonary iNKT cells can cause COPD-like symptoms [37], after adoptive transfer of iNKT cells in a mouse model of ischemia-reperfusion injury, the lung injury score was increased by H&E [36]. The above studies suggest that iNKT cells activation and recruitment can aggravate lung injury, but whether it affects AEC II differentiation needs to be further studied.

AEC II is the main stem cell in the lung, which can differentiate into AEC I [5]. In BPD, AEC II plays a central role in lung development arrest and injury repair. In our study, after 72 h of hyperoxia exposure, the expression of SP-C decreased, and T1α increased. The expression of T1α is different in vivo and in vitro under hyperoxia, which may be related to the following reasons: firstly, environment is not the same in vivo and in vitro, in vivo, cells are affected by many factors, including signal transduction between cells, immune response, etc., while in vitro culture, the cell environment is relatively simplified, may lead to different response patterns; secondly, the length of hyperoxia exposure is also different, 72 h of hyperoxia exposure is an acute lung injury, T1α compensatory increase. 14 days of hyperoxia exposure is a chronic lung injury, T1α decompensatory decrease, this is consistent with the results of Cao YX et al. [53] and Hou A et al. [54]; thirdly, Yee M et al., found that the increased T1α under hyperoxia is not differentiated from the labeled AEC II by special labeling of AEC II [55]. In future studies, tracing techniques for AEC II can be combined to better understand the functional changes of AEC II. To further clarify the effect of iNKT cells on AEC II, we verified it at the cellular level. We constructed AEC II-iNKT cells co-culture system by transwell technology and under hyperoxia exposure. Immunofluorescence and WB results showed that SP-C decreased in the group of AEC II alone under hyperoxia, and the decrease of SP-C and T1α in the co-culture group of AEC II-iNKT cells was more significant under hyperoxia. Fluorescence localization showed that the co-localization of SP-C and T1α in AEC II-iNKT cells co-cultured under hyperoxia was decreased, suggesting that iNKT cells aggravated abnormal AEC II under hyperoxia.

Next, to explore the possible mechanisms underlying the effect of iNKT cells on AEC II, we performed RNA

sequencing of AEC II in different groups, DEGs with PCD in the GO database related genes are compared, we found that among all PCD related differential genes, the number of DEGs related to ferroptosis was the highest. Ferroptosis is a form of PCD that is induced by lipid peroxidation and is iron-dependent [12,56,57], which plays an important role in the molecular and biological mechanism of BPD [58]. Previous studies have shown that hyperoxia induces ferroptosis and impairs lung development in neonatal mice, and features of ferroptosis are detected in mouse lung tissues and in vitro cell models under hyperoxia conditions [58]. Ferroptosis induces alveolar type II cell damage [59], induces epithelial-mesenchymal transition (EMT) in alveolar epithelial cells and promotes the process of fibrosis [60,61]. Recent studies also found that ferroptosis in AEC II causes pathological damage under hyperoxia and other stimuli. Additionally, ferroptosis is considered immune-regulated, and immune-derived cell death [62]. Gpx4 is the main core enzyme regulating the glutathione antioxidant system, and its reduction is an important marker for the occurrence of ferroptosis [56]. Our current study shows ferroptosis was changed both in AEC II cultured alone under hyperoxia and AEC II-iNKT cells co-cultured under hyperoxia, but more pronounced in AEC II-iNKT cells co-cultured group under hyperoxia, these changes included increased Fe^{2+}, Lipid peroxidation, and MDA levels, as well as elevated expression of genes PTGS2, reduced expression of GPX4 and FTH1, and ferroptosis characteristics were more obvious in AEC II-iNKT cells co-cultured group by transmission electron microscopy. However, whether iNKT cells recruitment and activation aggravates AEC II abnormal differentiation by ferroptosis need further study. To further demonstrate that iNKT cells aggravate AEC II damage by inducing ferroptosis under hyperoxia, ferroptosis activator Erastin and ferroptosis inhibitor Fer-1 were used. We found that T1α and SP-C were decreased when Erastin were added in iNKT + AEC II group, after add ferroptosis inhibitor Fer-1, showed that T1α and SP-C were increased, these suggested that AEC II ferroptosis accompanied by decreased expression of SP-C and T1α. Previous studies have found that hyperoxia promotes AEC II ferroptosis, and increases the transdifferentiation of type II epithelial cells into mesenchymal-like cells [63]. Ferroptosis inhibitors liproxstatin - 1 (Lip) and deferoxamine (DFO) alleviated the symptoms of pulmonary fibrosis [64]. These studies suggested that increased ferroptosis realates to differentation of AEC II. Our study mainly showed that iNKT cells aggravated the ferroptosis of AEC II under hyperoxia, but the specific mechanism still needs to be further studied. Previous studies have shown that IL-17A promotes airway epithelial ferroptosis in asthma [65], and it has been reported that IL-17A can cooperate with IL-6 to promote ferroptosis of alveolar epithelial cells under acute hyperoxia [66]. Previous study found that the pro-inflammatory effect of iNKT cells was mainly through the secretion of IL-17A and IL-6. Co-culture of AEC II and iNKT cells increased IL-17A levels than only AEC II cultured alone. Some studies reported the IL - 6 in the expression and significance of BPD environment [67]. After specifically activating iNKT cells, we found that inflammatory factor IL-6 and IL-17A were increased in vivo, IL-17A and IL-6 were also increased in the supernatant of AEC II-iNKT cells co-cultured in vitro under hyperoxia. Therefore, we speculate that iNKT cells may also promote ferroptosis in AEC II by secreting IL-17A together with IL-6 present in the inflammatory environment. However, we have only initially explored the mechanism by which iNKT cells affect abnormal AEC II expression under hyperoxia. For this is just our speculation and some preliminary experimental verification, the follow-up still need further study.

Nevertheless, there are still some limitations in this study. Our current study only found that iNKT cells affected the

expression of AEC II and AEC I after hyperoxia, there is no direct evidence to support an association between the abundance and activation iNKT cells with impaired differentiation of AEC II into AEC I. Our study only used single gene to represent AEC II or AEC I to investigate the differentiation, we only use SP-C and T1α as the gene marker, if use multiple gene markers may be more rigorous. In future experiments, we will also employ lineage label to more clearly observe AEC II differentiation status in different pathological environments. Certainly, the most specific tool for iNKT cells in mice and humans are αGalCer/CD1d tetramers, it may be more specific if αGalCer/CD1d tetramers are employed. In addition, the main pathological manifestations of BPD are alveolarization disorder and abnormal pulmonary microvascular development, the interaction between NKT cells and pulmonary microvascular endothelial cells under hyperoxia has not been explored. Studies have found that peripheral blood NKT cells are increased and activated, and inhibit the proliferation and migration of human umbilical vein endothelial cells (HUVECs), thereby inducing vascular injuries in diabetes [68]. S K et al. found that NKT cells induced by IL-4 leads to pulmonary artery wall thickening [69]. These studies suggested that abnormal activation of NKT cells may also affect microvascular endothelial cells, however, further studies are needed to determine whether NKT cells affects pulmonary microvascular development in BPD.

Studies showed that iNKT cells accumulate mainly in microvasculature after moving from the thymus into circulation, and there is substantial evidence that iNKT cells migration into the lung tissue rapidly under various activation conditions, such as when the lung is stimulated by airborne antigens or infections [14]. Based on the above and our experimental results, can only presume hyperoxia lead to an increased recruitment or local expansion of activated iNKT cells in the lungs, which cannot be accurately determined as recruitment or tissue resident. In addition, CD69 in iNKT cells was detected to be elevated, and it is also one of the markers of early activation and tissue resident lymphocytes, however, an increase in CD69 alone does not represent tissue resident cells, may need to be confirmed by parabiosis experiments [70], so, we still need more in-depth research, and these will be further studied in the future.

Our study found that hyperoxia leads to the recruitment and activation of iNKT cells in the lungs. Over-activated iNKT cells induces ferroptosis in AEC II, accompanied by decreased expression of SP-C and T1α. AEC II dysfunction leads to the obstruction of alveolarization and occurrence of BPD.

Ethics approval and consent to participate

The study was approved by the Biomedical Research Ethics Committee of the Affiliated Hospital of Jiangsu University (SWYXLL20200121-17). The animal procedures were approved by the Institutional Animal Care and Use Committee of Jiangsu University (Grant no: UJS-IACUC-AP-2022052501) (Supplementary Fig. 2).

Availability of data and materials

The datasets used and/or analyzed during the current study are available from the corresponding author on reasonable request.

Funding

We are particularly grateful to the participants in this research.

Funding: This study was supported by National Natural Science Foundation of China (No.82171702), Zhenjiang Science and Technology Innovation Funds - Clinical Medicine Key Laboratory (SS2023012), Scientific Research Project of Health Commission of Jiangsu Province (M2022043), and Graduate student research and creative projects of Jiangsu Province (grant No. KYCX23_3755).

CRediT authorship contribution statement

Ming-Yan Wang: Writing – review & editing, Writing – original draft, Visualization, Software, Methodology, Funding acquisition. **Meng-Xu Yi:** Validation, Software, Resources, Data curation. **Xing-Yu Mo:** Validation, Software, Resources, Data curation. **Shan-Jie Wei:** Software, Resources, Methodology, Investigation. **Yu Qiao:** Resources, Investigation, Formal analysis, Data curation. **Zheng Zhang:** Visualization, Software, Resources. **Zhao-Liang Su:** Writing – review & editing, Supervision, Methodology. **Hong-Yan Lu:** Writing – review & editing, Supervision, Project administration, Funding acquisition, Conceptualization.

Declaration of competing interest

The authors declare that they have no known competing financial interests or personal relationships that could have appeared to influence the work reported in this paper.

Acknowledgements

Not applicable.

Footnotes

Appendix A Supplementary data to this article can be found online at https://doi.org/10.1016/j.redox.2024.103370 .

Contributor Information

Zhao-Liang Su, Email: szl30@ujs.edu.cn.

Hong-Yan Lu, Email: hylu@ujs.edu.cn.

Appendix A. Supplementary data

The following are the Supplementary data to this article:

Multimedia component 1

mmc1.docx (2.4MB, docx)

Data availability

Data will be made available on request.

References

1. Principi N., Di Pietro G.M., Esposito S. Bronchopulmonary dysplasia: clinical aspects and preventive and therapeutic strategies. J. Transl. Med. 2018;16(1):36. doi: 10.1186/s12967-018-1417-7. [DOI] [PMC free article] [PubMed] [Google Scholar]

2. Bancalari E., Jain D. Bronchopulmonary dysplasia: 50 Years after the original description. Neonatology. 2019;115(4):384–391. doi: 10.1159/000497422. [DOI] [PubMed] [Google Scholar]

3. Hurskainen M., Mizikova I., Cook D.P., et al. Single cell transcriptomic analysis of murine lung development on hyperoxia-induced damage. Nat. Commun. 2021;12(1):1565. doi: 10.1038/s41467-021-21865-2. [DOI] [PMC free article] [PubMed] [Google Scholar]

4. Hogan B.L., Barkauskas C.E., Chapman H.A., et al. Repair and regeneration of the respiratory system: complexity, plasticity, and mechanisms of lung stem cell function. Cell Stem Cell. 2014;15(2):123–138. doi: 10.1016/j.stem.2014.07.012. [DOI] [PMC free article] [PubMed] [Google Scholar]

5. Wang Y., Tang Z., Huang H., et al. Pulmonary alveolar type I cell population consists of two distinct subtypes that differ in cell fate. Proc Natl Acad Sci U S A. 2018;115(10):2407–2412. doi: 10.1073/pnas.1719474115. [DOI] [PMC free article] [PubMed] [Google Scholar]

6. Langyue H., Ying Z., Jianfeng J., et al. IRF4-mediated Treg phenotype switching can aggravate hyperoxia-induced alveolar epithelial cell injury. BMC Pulm. Med. 2024;24(1):130. doi: 10.1186/s12890-024-02940-y. [DOI] [PMC free article] [PubMed] [Google Scholar]

7. Lignelli E., Palumbo F., Myti D., et al. Recent advances in our understanding of the mechanisms of lung alveolarization and bronchopulmonary dysplasia. Am. J. Physiol. Lung Cell Mol. Physiol. 2019;317(6):L832–L887. doi: 10.1152/ajplung.00369.2019. [DOI] [PubMed] [Google Scholar]

8. Lu H., Chen X., Lu Y., et al. Effects of C/EBPalpha overexpression on alveolar epithelial type II cell proliferation, apoptosis and surfactant protein-C expression after exposure to hyperoxia. BMC Pulm. Med. 2019;19(1):142. doi: 10.1186/s12890-019-0911-x. [DOI] [PMC free article] [PubMed] [Google Scholar]

9. Liao J., Kapadia V.S., Brown L.S., et al. The NLRP3 inflammasome is critically involved in the development of bronchopulmonary dysplasia. Nat. Commun. 2015;6:8977. doi: 10.1038/ncomms9977. [DOI] [PMC free article] [PubMed] [Google Scholar]

10. Zhang L., Soni S., Hekimoglu E., et al. Impaired autophagic activity contributes to the pathogenesis of bronchopulmonary dysplasia. Evidence from murine and baboon models. Am. J. Respir. Cell Mol. Biol. 2020;63(3):338–348. doi: 10.1165/rcmb.2019-0445OC. [DOI] [PMC free article] [PubMed] [Google Scholar]

11. Chou H.C., Chen C.M. Cathelicidin attenuates hyperoxia-induced lung injury by inhibiting ferroptosis in newborn rats. Antioxidants. 2022;11(12) doi: 10.3390/antiox11122405. [DOI] [PMC free article] [PubMed] [Google Scholar]

12. Deng X., Bao Z., Yang X., et al. Molecular mechanisms of cell death in bronchopulmonary dysplasia. Apoptosis. 2023;28(1–2):39–54. doi: 10.1007/s10495-022-01791-4. [DOI] [PubMed] [Google Scholar]

13. Lao J.C., Bui C.B., Pang M.A., et al. Type 2 immune polarization is associated with cardiopulmonary disease in preterm infants. Sci. Transl. Med. 2022;14(639) doi: 10.1126/scitranslmed.aaz8454. [DOI] [PubMed] [Google Scholar]

14. Jeong D., Woo Y.D., Chung D.H. Invariant natural killer T cells in lung diseases. Exp. Mol. Med. 2023;55(9):1885–1894. doi: 10.1038/s12276-023-01024-x. [DOI] [PMC free article] [PubMed] [Google Scholar]

15. Jia H., Chen J., Zhang X., et al. IL-17A produced by invariant natural killer T cells and CD3(+) CD56(+)

alphaGalcer-CD1d tetramer(-) T cells promote liver fibrosis in patients with primary biliary cholangitis. J. Leukoc. Biol. 2022;112(5):1079–1087. doi: 10.1002/JLB.2A0622-586RRRR. [DOI] [PubMed] [Google Scholar]

16. Kumar V., Hertz M., Agro A., et al. Type 1 invariant natural killer T cells in chronic inflammation and tissue fibrosis. Front. Immunol. 2023;14 doi: 10.3389/fimmu.2023.1260503. [DOI] [PMC free article] [PubMed] [Google Scholar]

17. Lee Y.J., Wang H., Starrett G.J., et al. Tissue-specific distribution of iNKT cells impacts their cytokine response. Immunity. 2015;43(3):566–578. doi: 10.1016/j.immuni.2015.06.025. [DOI] [PMC free article] [PubMed] [Google Scholar]

18. Cui G., Shimba A., Jin J., et al. A circulating subset of iNKT cells mediates antitumor and antiviral immunity. Sci Immunol. 2022;7(76) doi: 10.1126/sciimmunol.abj8760. [DOI] [PubMed] [Google Scholar]

19. Crosby C.M., Kronenberg M. Tissue-specific functions of invariant natural killer T cells. Nat. Rev. Immunol. 2018;18(9):559–574. doi: 10.1038/s41577-018-0034-2. [DOI] [PMC free article] [PubMed] [Google Scholar]

20. Victor J.R., Lezmi G., Leite-de-Moraes M. New insights into asthma inflammation: focus on iNKT, MAIT, and gammadeltaT cells. Clin. Rev. Allergy Immunol. 2020;59(3):371–381. doi: 10.1007/s12016-020-08784-8. [DOI] [PubMed] [Google Scholar]

21. Pichavant M., Remy G., Bekaert S., et al. Oxidative stress-mediated iNKT-cell activation is involved in COPD pathogenesis. Mucosal Immunol. 2014;7(3):568–578. doi: 10.1038/mi.2013.75. [DOI] [PMC free article] [PubMed] [Google Scholar]

22. Zou L., Dang W., Tao Y., et al. The il-33/st2 Axis promotes acute respiratory distress syndrome by natural killer T cells. Shock. 2023;59(6):902–911. doi: 10.1097/SHK.0000000000002114. [DOI] [PMC free article] [PubMed] [Google Scholar]

23. Brennan P.J., Brigl M., Brenner M.B. Invariant natural killer T cells: an innate activation scheme linked to diverse effector functions. Nat. Rev. Immunol. 2013;13(2):101–117. doi: 10.1038/nri3369. [DOI] [PubMed] [Google Scholar]

24. Fallon E.A., Chun T.T., Young W.A., et al. Program cell death receptor-1-mediated invariant natural killer T-cell control of peritoneal macrophage modulates survival in neonatal sepsis. Front. Immunol. 2017;8:1469. doi: 10.3389/fimmu.2017.01469. [DOI] [PMC free article] [PubMed] [Google Scholar]

25. Lee S.Y., Noh Y., Goo J.H., et al. Natural killer T cell sensitization during neonatal respiratory syncytial

virus infection induces eosinophilic lung disease in re-infected adult mice. PLoS One. 2017;12(6) doi: 10.1371/journal.pone.0176940. [DOI] [PMC free article] [PubMed] [Google Scholar]

26. Gordy L.E., Bezbradica J.S., Flyak A.I., et al. IL-15 regulates homeostasis and terminal maturation of NKT cells. J. Immunol. 2011;187(12):6335–6345. doi: 10.4049/jimmunol.1003965. [DOI] [PMC free article] [PubMed] [Google Scholar]

27. Pietrzyk J.J., Kwinta P., Wollen E.J., et al. Gene expression profiling in preterm infants: new aspects of bronchopulmonary dysplasia development. PLoS One. 2013;8(10) doi: 10.1371/journal.pone.0078585. [DOI] [PMC free article] [PubMed] [Google Scholar]

28. Higgins R.D., Jobe A.H., Koso-Thomas M., et al. Bronchopulmonary dysplasia: executive summary of a workshop. J. Pediatr. 2018;197:300–308. doi: 10.1016/j.jpeds.2018.01.043. [DOI] [PMC free article] [PubMed] [Google Scholar]

29. Jandl K., Marsh L.M., Mutgan A.C., et al. Impairment of the NKT-STAT1-CXCL9 Axis contributes to vessel fibrosis in pulmonary hypertension caused by lung fibrosis. Am. J. Respir. Crit. Care Med. 2022;206(8):981–998. doi: 10.1164/rccm.202201-0142OC. [DOI] [PubMed] [Google Scholar]

30. Lin B., Jia X., Xie Z., et al. Vascular endothelial cells activate peripheral natural killer T cells and participate in regulation of downstream immune cascades in patients with sepsis. Med. Sci. Mon. Int. Med. J. Exp. Clin. Res. 2018;24:7387–7398. doi: 10.12659/MSM.911466. [DOI] [PMC free article] [PubMed] [Google Scholar]

31. Zhu Y., Yao H.C., Lu H.Y., et al. IL-33-ST2 pathway regulates AECII transdifferentiation by targeting alveolar macrophage in a bronchopulmonary dysplasia mouse model. J. Cell Mol. Med. 2023;27(2):304–308. doi: 10.1111/jcmm.17654. [DOI] [PMC free article] [PubMed] [Google Scholar]

32. Yang M., Chen Y., Huang X., et al. Lysine demethylase KDM3A alleviates hyperoxia-induced bronchopulmonary dysplasia in mice by promoting ETS1 expression. Exp. Cell Res. 2024;435(2) doi: 10.1016/j.yexcr.2024.113945. [DOI] [PubMed] [Google Scholar]

33. Zhu Y., Mi L., Lu H., et al. ILC2 regulates hyperoxia-induced lung injury via an enhanced Th17 cell response in the BPD mouse model. BMC Pulm. Med. 2023;23(1):188. doi: 10.1186/s12890-023-02474-9. [DOI] [PMC free article] [PubMed] [Google Scholar]

34. Rijavec M., Volarevic S., Osolnik K., et al. Natural killer T cells in pulmonary disorders. Respir. Med. 2011;105(Suppl 1):S20–S25. doi: 10.1016/S0954-6111(11)70006-3. [DOI] [PubMed] [Google Scholar]

35. Cha H., Qin W., Yang Q., et al. Differential pulmonic NK and NKT cell responses in Schistosoma japonicum-infected mice. Parasitol. Res. 2017;116(2):559–567. doi: 10.1007/s00436-016-5320-y. [DOI]

[PubMed] [Google Scholar]

36. Wallace K.L., Marshall M.A., Ramos S.I., et al. NKT cells mediate pulmonary inflammation and dysfunction in murine sickle cell disease through production of IFN-gamma and CXCR3 chemokines. Blood. 2009;114(3):667–676. doi: 10.1182/blood-2009-02-205492. [DOI] [PMC free article] [PubMed] [Google Scholar]

37. Tsao C.C., Tsao P.N., Chen Y.G., et al. Repeated activation of lung invariant NKT cells results in chronic obstructive pulmonary disease-like symptoms. PLoS One. 2016;11(1) doi: 10.1371/journal.pone.0147710. [DOI] [PMC free article] [PubMed] [Google Scholar]

38. Hong J.R., Zhang C.Y., Zhong W.J., et al. Epoxyeicosatrienoic acids alleviate alveolar epithelial cell senescence by inhibiting mitophagy through NOX4/Nrf2 pathway. Biomed. Pharmacother. 2023;169 doi: 10.1016/j.biopha.2023.115937. [DOI] [PubMed] [Google Scholar]

39. Ridsdale R., Post M. Surfactant lipid synthesis and lamellar body formation in glycogen-laden type II cells. Am. J. Physiol. Lung Cell Mol. Physiol. 2004;287(4):L743–L751. doi: 10.1152/ajplung.00146.2004. [DOI] [PubMed] [Google Scholar]

40. Thebaud B., Goss K.N., Laughon M., et al. Bronchopulmonary dysplasia. Nat. Rev. Dis. Prim. 2019;5(1):78. doi: 10.1038/s41572-019-0127-7. [DOI] [PMC free article] [PubMed] [Google Scholar]

41. Fehrenbach H. Alveolar epithelial type II cell: defender of the alveolus revisited. Respir. Res. 2001;2(1) doi: 10.1186/rr36. [DOI] [PMC free article] [PubMed] [Google Scholar]

42. Lim K., Rawlins E.L. Protocol for the derivation and alveolar type 2 differentiation of late-stage lung tip progenitors from the developing human lungs. STAR Protoc. 2024;5(3) doi: 10.1016/j.xpro.2024.103201. [DOI] [PubMed] [Google Scholar]

43. Liebler J.M., Marconett C.N., Juul N., et al. Combinations of differentiation markers distinguish subpopulations of alveolar epithelial cells in adult lung. Am. J. Physiol. Lung Cell Mol. Physiol. 2016;310(2):L114–L120. doi: 10.1152/ajplung.00337.2015. [DOI] [PMC free article] [PubMed] [Google Scholar]

44. Whitsett J.A., Weaver T.E. Hydrophobic surfactant proteins in lung function and disease. N. Engl. J. Med. 2002;347(26):2141–2148. doi: 10.1056/NEJMra022387. [DOI] [PubMed] [Google Scholar]

45. Koh J., Woo Y.D., Yoo H.J., et al. De novo fatty-acid synthesis protects invariant NKT cells from cell death, thereby promoting their homeostasis and pathogenic roles in airway hyperresponsiveness. Elife. 2023;12 doi: 10.7554/eLife.87536. [DOI] [PMC free article] [PubMed] [Google Scholar]

46. Nowak-Machen M., Schmelzle M., Hanidziar D., et al. Pulmonary natural killer T cells play an essential

role in mediating hyperoxic acute lung injury. Am. J. Respir. Cell Mol. Biol. 2013;48(5):601–609. doi: 10.1165/rcmb.2012-0180OC. [DOI] [PMC free article] [PubMed] [Google Scholar]

47. Aoyagi T., Yamamoto N., Hatta M., et al. Activation of pulmonary invariant NKT cells leads to exacerbation of acute lung injury caused by LPS through local production of IFN-gamma and TNF-alpha by Gr-1+ monocytes. Int. Immunol. 2011;23(2):97–108. doi: 10.1093/intimm/dxq460. [DOI] [PubMed] [Google Scholar]

48. Bedard M., Shrestha D., Priestman D.A., et al. Sterile activation of invariant natural killer T cells by ER-stressed antigen-presenting cells. Proc Natl Acad Sci U S A. 2019;116(47):23671–23681. doi: 10.1073/pnas.1910097116. [DOI] [PMC free article] [PubMed] [Google Scholar]

49. Szabo P.A., Rudak P.T., Choi J., et al. Invariant natural killer T cells are pathogenic in the HLA-DR4-transgenic humanized mouse model of toxic shock syndrome and can Be targeted to reduce morbidity. J. Infect. Dis. 2017;215(5):824–829. doi: 10.1093/infdis/jiw646. [DOI] [PubMed] [Google Scholar]

50. Liu B., Jiang J., Liang H., et al. Natural killer T cell/IL-4 signaling promotes bone marrow-derived fibroblast activation and M2 macrophage-to-myofibroblast transition in renal fibrosis. Int Immunopharmacol. 2021;98 doi: 10.1016/j.intimp.2021.107907. [DOI] [PubMed] [Google Scholar]

51. Ishikawa S., Ikejima K., Yamagata H., et al. CD1d-restricted natural killer T cells contribute to hepatic inflammation and fibrogenesis in mice. J. Hepatol. 2011;54(6):1195–1204. doi: 10.1016/j.jhep.2010.08.022. [DOI] [PubMed] [Google Scholar]

52. Chen D., Xu W., Teng J., et al. Migration, distribution, and safety evaluation of specific phenotypic and functional mouse spleen-derived invariant natural killer T2 cells after adoptive infusion. Mediat. Inflamm. 2021;2021 doi: 10.1155/2021/5170123. [DOI] [PMC free article] [PubMed] [Google Scholar]

53. Cao Y.X., Ramirez M.I., Williams M.C. Enhanced binding of Sp1/Sp3 transcription factors mediates the hyperoxia-induced increased expression of the lung type I cell gene T1alpha. J. Cell. Biochem. 2003;89(5):887–901. doi: 10.1002/jcb.10555. [DOI] [PubMed] [Google Scholar]

54. Hou A., Fu J., Yang H., et al. Hyperoxia stimulates the transdifferentiation of type II alveolar epithelial cells in newborn rats. Am. J. Physiol. Lung Cell Mol. Physiol. 2015;308(9):L861–L872. doi: 10.1152/ajplung.00099.2014. [DOI] [PubMed] [Google Scholar]

55. Yee M., Buczynski B.W., O'Reilly M.A. Neonatal hyperoxia stimulates the expansion of alveolar epithelial type II cells. Am. J. Respir. Cell Mol. Biol. 2014;50(4):757–766. doi: 10.1165/rcmb.2013-0207OC. [DOI] [PMC free article] [PubMed] [Google Scholar]

56. Xie Y., Hou W., Song X., et al. Ferroptosis: process and function. Cell Death Differ. 2016;23(3):369–379.

doi: 10.1038/cdd.2015.158. [DOI] [PMC free article] [PubMed] [Google Scholar]

57. Dixon S.J., Lemberg K.M., Lamprecht M.R., et al. Ferroptosis: an iron-dependent form of nonapoptotic cell death. Cell. 2012;149(5):1060–1072. doi: 10.1016/j.cell.2012.03.042. [DOI] [PMC free article] [PubMed] [Google Scholar]

58. Chou H.C., Chen C.M. Hyperoxia induces ferroptosis and impairs lung development in neonatal mice. Antioxidants. 2022;11(4) doi: 10.3390/antiox11040641. [DOI] [PMC free article] [PubMed] [Google Scholar]

59. Cheng H.P., Feng D.D., Li X.H., et al. NMDA receptor activation induces damage of alveolar type II cells and lung fibrogenesis through ferroptosis. Biochim. Biophys. Acta Mol. Cell Res. 2023;1870(7) doi: 10.1016/j.bbamcr.2023.119535. [DOI] [PubMed] [Google Scholar]

60. Ling H., Xiao H., Luo T., et al. Role of ferroptosis in regulating the epithelial-mesenchymal transition in pulmonary fibrosis. Biomedicines. 2023;11(1) doi: 10.3390/biomedicines11010163. [DOI] [PMC free article] [PubMed] [Google Scholar]

61. Takahashi M., Mizumura K., Gon Y., et al. Iron-dependent mitochondrial dysfunction contributes to the pathogenesis of pulmonary fibrosis. Front. Pharmacol. 2021;12 doi: 10.3389/fphar.2021.643980. [DOI] [PMC free article] [PubMed] [Google Scholar]

62. Chen X., Kang R., Kroemer G., et al. Ferroptosis in infection, inflammation, and immunity. J. Exp. Med. 2021;218(6) doi: 10.1084/jem.20210518. [DOI] [PMC free article] [PubMed] [Google Scholar]

63. Yue D., Zhang Q., Zhang J., et al. Diesel exhaust PM2.5 greatly deteriorates fibrosis process in pre-existing pulmonary fibrosis via ferroptosis. Environ. Int. 2023;171 doi: 10.1016/j.envint.2022.107706. [DOI] [PubMed] [Google Scholar]

64. Pei Z., Qin Y., Fu X., et al. Inhibition of ferroptosis and iron accumulation alleviates pulmonary fibrosis in a bleomycin model. Redox Biol. 2022;57 doi: 10.1016/j.redox.2022.102509. [DOI] [PMC free article] [PubMed] [Google Scholar]

65. Song J., Zhang H., Tong Y., et al. Molecular mechanism of interleukin-17A regulating airway epithelial cell ferroptosis based on allergic asthma airway inflammation. Redox Biol. 2023;68 doi: 10.1016/j.redox.2023.102970. [DOI] [PMC free article] [PubMed] [Google Scholar]

66. Guo B., Zuo Z., Di X., et al. Salidroside attenuates HALI via IL-17A-mediated ferroptosis of alveolar epithelial cells by regulating Act1-TRAF6-p38 MAPK pathway. Cell Commun. Signal. 2022;20(1):183. doi: 10.1186/s12964-022-00994-1. [DOI] [PMC free article] [PubMed] [Google Scholar]

67. Hirani D., Alvira C.M., Danopoulos S., et al. Macrophage-derived IL-6 trans-signalling as a novel target in the pathogenesis of bronchopulmonary dysplasia. Eur. Respir. J. 2022;59(2) doi: 10.1183/13993003.02248-2020. [DOI] [PMC free article] [PubMed] [Google Scholar]

68. Lv X., Gao Y., Dong T., et al. Role of natural killer T (NKT) cells in type II diabetes-induced vascular injuries. Med. Sci. Mon. Int. Med. J. Exp. Clin. Res. 2018;24:8322–8332. doi: 10.12659/MSM.912446. [DOI] [PMC free article] [PubMed] [Google Scholar]

69. Kawashima S., Hirose K., Takahashi K., et al. Interleukin-25 induces pulmonary arterial remodeling via natural killer T cell-dependent mechanisms. Int. Arch. Allergy Immunol. 2013;161(Suppl. 2):118–124. doi: 10.1159/000350379. [DOI] [PubMed] [Google Scholar]

70. Yang C., Liu Z.L., Wang J., et al. Parabiosis modeling: protocol, application and perspectives. Zool. Res. 2021;42(3):253–261. doi: 10.24272/j.issn.2095-8137.2020.368. [DOI] [PMC free article] [PubMed] [Google Scholar]

Associated Data

This section collects any data citations, data availability statements, or supplementary materials included in this article.

Supplementary Materials

Multimedia component 1

mmc1.docx (2.4MB, docx)

Data Availability Statement

The datasets used and/or analyzed during the current study are available from the corresponding author on reasonable request.

Data will be made available on request.